

# **PDielec: The Calculation of Infrared and Terahertz Absorption for Powdered Crystals**

John Kendrick<sup>1</sup> and Andrew Burnett<sup>1</sup>

<sup>1</sup>School of Chemistry, University of Leeds, Leeds, LS2 9JT United Kingdom.

## **ABSTRACT**

The Python package PDielec is described, which calculates the infrared absorption characteristics of a crystalline material supported in a non-absorbing medium. PDielec post processes solid state quantum mechanical and molecular mechanical calculations of the phonons and dielectric response of the crystalline material. Packages supported are; Abinit, Castep, Crystal14, Gulp, QuantumEspresso, Phonopy and VASP. Using an effective medium method, the package calculates the internal electric field arising from different particle morphologies and calculates the resulting shift in absorption frequency and intensity arising from the coupling between a phonon and the internal field. The theory of the approach is described, followed by a description of the implementation within PDielec. For the specific case of a low concentration of spherical particles, calculations based on Mie scattering allow the exploration of particle size effects. A section providing several examples of its application is given.

## **INTRODUCTION**

The molecular and solid state quantum mechanical (QM) calculations of response properties such as the frequencies and intensities of infrared (IR) and terahertz (THz) radiation absorption has become generally available in many molecular and solid state computer programs. A common approach is to assume the harmonic approximation and calculate the mass weighted force constant matrix (for molecules) or the dynamical matrix at the gamma point (for periodic solids). Diagonalisation of the matrix gives the frequencies for absorption and the normal modes (molecules) or phonon displacements (periodic solids). The calculation of the absorption intensity for each mode requires the calculation of the change in dipole moment caused by the displacement of the atoms for that mode. For solids where there is a large separation of charge, there can be a large coupling between a phonon mode and the internal field within a particle resulting from its morphology. This paper describes the PDielec package, which is written in Python and post processes the output of solid state quantum mechanical and molecular mechanics (MM) based codes such as VASP,<sup>1</sup> CASTEP<sup>2</sup>, CRYSTAL<sup>3</sup>, Abinit<sup>4</sup>, and Quantum Espresso<sup>5</sup>, Phonopy<sup>6</sup>, and GULP<sup>7</sup> to predict the infrared absorption of crystalline insulator materials whose crystal size is small compared with the wavelength of the absorbing radiation. The package is suited for the calculation of the complex, frequency dependent permittivity and its associated absorption of infrared radiation for a finely ground crystalline material dispersed in a low loss dielectric medium such KBr or Polytetrafluoroethylene (PTFE). A particular feature of the program is its ability to take into account the constant permittivity of the supporting medium and the particle shape of the material of interest through an effective medium theory. The

paper outlines the theory used by the program and gives some examples of the application of the program for ionic and molecular materials.

## THEORY

Equation 1 describes Beer-Lambert's law<sup>8</sup> where  $\alpha$  is the (decadic) absorption coefficient (usually given in  $\text{cm}^{-1}$ ),  $I$  and  $I_0$  are the intensities after and before absorption respectively and  $d$  is the path length.

$$\frac{I}{I_0} = 10^{-\alpha d}$$

$$-\log \left( \frac{I}{I_0} \right) = \alpha d$$
Equation 1

It is common, especially in the chemistry community, when reporting infrared spectra to use a decadic molar absorption coefficient ( $a$ ), which has units of  $\text{L}\cdot\text{mol}^{-1}\text{cm}^{-1}$ . The relationship between the absorption coefficient and the molar absorption coefficient<sup>8</sup> is;

$$\alpha = aC$$
Equation 2

where  $C$  is the concentration of the absorbing species.

### Molecular Approach to Absorption Intensity

For molecules the transition intensity  $I_k$  of the  $k^{\text{th}}$  mode (calculated from the change in dipole moment along the mode displacement) can be converted to an integrated molar absorption coefficient,  $A_k$ , which can then be more readily compared with experiment. The theory for this is described by Wilson, Decius and Cross<sup>9</sup> and results in expressions such as the two equations below (Equation 3). The first expression shows the relationship between the integrated molar absorption coefficient and the transition intensity and uses the number of molecules per unit volume ( $N$ ), the velocity of light ( $c$ ) and the degeneracy of the mode ( $g_k$ ). The second expression shows the appropriate conversion factors if the units for the integrated molar absorption coefficient are  $\text{L}\cdot\text{mol}^{-1}\text{cm}^{-2}$  ( $1 \text{ L}\cdot\text{mol}^{-1}\text{cm}^{-2} = 0.01 \text{ km}\cdot\text{mol}^{-1}$ ) and the units for the transition intensity are  $\text{D}^2\cdot\text{\AA}^{-2}\cdot\text{amu}^{-1}$ , where D represents the Debye unit of dipole moment and amu is an atomic mass unit. The factor  $\log_{10}$  arises due to the choice of a decadic Beer's law.

$$A_k = \frac{N\pi}{3c^2\log_{10}10} g_k I_k$$

$$A_k = \frac{N_a \pi}{300 c^2 2.3025} g_k I_k = 422 \cdot \tilde{g} I_k$$
Equation 3

The derivation of the above expressions assumes that the rotational levels are not quantised and that the vibrational levels are thermally occupied according to a Boltzmann distribution. In order to

use the calculated molecular intensities to predict a spectrum it is usual to assume<sup>9</sup> that each transition is associated with a Lorentzian line shape with a full width at half maximum (FWHM) of  $\sigma_k$ . It is common, when reporting comparison between theoretical and experimental spectra, to assume that the line widths are the same for all modes.<sup>10,11</sup> Recent work on terahertz absorption in crystalline pentaerythritol tetranitrate (PETN) using molecular dynamics calculations<sup>12</sup> in combination with the direct calculation of the cubic anharmonic couplings of the normal modes<sup>13</sup> has shown that the FWHM of the intense absorptions may vary between 10 and 25 cm<sup>-1</sup>. Assuming a Lorentzian line shape, the molar absorption coefficient for the  $k^{\text{th}}$  mode at wavenumber,  $\bar{v}_k$ , can be written as a function of frequency or wavenumber ( $\bar{v}$ );

$$a_k(\bar{v})_x = \frac{2A_k}{\pi} \frac{\sigma_k}{4(\bar{v} - \bar{v}_k)^2 + \sigma_k^2} \quad \text{Equation 4}$$

$$a_k^{\text{ma}} = \frac{2A_k}{\pi\sigma_k}$$

x

The maximum height of the Lorentzian,  $a_k^{\text{ma}}$ , clearly depends upon the value of  $\sigma_k$ . As can be seen in Equation 5, the choice of normalisation for the Lorentzian means that integration of the molar absorption coefficient over wavenumber returns the integrated molar absorption coefficient and a sum over all the bands provides the total molar absorption coefficient  $a^{mo}(\bar{v})$  as a function of wavenumber, calculated from the intensities of each band. The final expression in Equation 5 shows the relationship between the absorption and the molar absorption coefficients. C is the concentration usually expressed in mol/L.

$$A_k = \int a_k(\bar{v}) d\bar{v}$$

$$a^{mo}_l(\bar{v}) = \sum_k a_k(\bar{v}) \quad \text{Equation 5}$$

$$\alpha^{mo}(\bar{v}) = Ca^{mo}(\bar{v})$$

A comment should be made about the various units which can be used for these quantities. A common unit for the transition intensity is (D/Å)<sup>2</sup>/amu, another is km/mol. However, it should be pointed out that strictly speaking the latter unit refers to the integrated molar absorption coefficient as defined above in Equation 3 and therefore relies on the assumptions made in its derivation ( 1 (D/Å)<sup>2</sup>/amu is equivalent to 42.256 km/mol ).

### Solid State Approach to Absorption Intensity

The optical properties of a solid are determined by its complex, frequency dependent relative permittivity ( $\bar{\epsilon}(\bar{v})$ ) and in particular the imaginary refractive index component tensor,  $\bar{\kappa}$ , of the complex refractive index,  $\bar{\bar{N}}$  where;

$$\bar{\bar{N}}(\bar{v})^2 = \bar{\epsilon}(\bar{v}) \quad \text{Equation 6}$$

$$\bar{\bar{N}}(\bar{v}) = \bar{\bar{n}}(\bar{v}) + i\bar{\bar{\kappa}}(\bar{v})$$

The intensity of absorption is given by the effect of the imaginary component of the refractive index on the incident light assuming an isotropic material<sup>10</sup>;

$$\begin{aligned} I &= I_0 e^{-4\pi\kappa(\bar{v})d/\lambda} \\ I &= I_0 e^{-4\pi\bar{v}\kappa(\bar{v})d} \\ -\ln\left(\frac{I}{I_0}\right) &= 4\pi\bar{v}\kappa(\bar{v})d \quad g \\ -\ln\left(\frac{I}{I_0}\right) &= 4\pi\bar{v}\kappa(\bar{v})d \cdot \ln e \end{aligned} \quad \text{Equation 7}$$

Comparison with the definition of the absorption coefficient from Beer-Lambert's law (Equation 1) gives;

$$\begin{aligned} \alpha^{so}_l(\bar{v}) &= 4\pi\bar{v}\kappa(\bar{v}) \cdot \ln e \\ \alpha^{so}(\bar{v}) &= \frac{\alpha^{so}(\bar{v})}{C} \end{aligned} \quad \text{Equation 8}$$

Since the refractive index is dimensionless, the absorption coefficient ( $\alpha^{so}$ ) is specified in  $\text{cm}^{-1}$ . The superscripts 'sol,' for solid, and 'mol,' for molecular, are used here to distinguish between the two methods of calculating the absorption ( $\alpha$ ) and molar absorption coefficients ( $a$ ). In the calculation of the imaginary component of the refractive index it is necessary to choose the solution which gives a positive value. This is consistent with the Kramers-Kronig relationship between the real and imaginary components.<sup>15</sup>

In order to calculate the relationship between absorption and molar absorption coefficients it is necessary to know the concentration. For solid state calculations the required unit is; moles of unit cells per litre. One of the drawbacks of this molar absorption coefficient unit is that the number of molecules in a unit cell can change depending on whether a supercell, primitive or non primitive unit cell is being used. A more natural unit would be to use a mole of formula units, or a mole of molecules. In order to aid comparison between such calculations PDielec is able to calculate concentration in both moles of atoms and moles of molecules. However for the rest of this paper Equation 9 will be used, where  $V$  is the volume of the unit cell, and therefore the concentration  $C$  is moles of unit cell/litre.

$$C = \frac{f \cdot 100 \text{ cm}^3}{VN_a} \quad \text{Equation 9}$$

The volume fraction,  $f$ , of the dielectric material in a supporting matrix of non-absorbing material is included in the expression for the concentration as it will be useful when the theory for mixtures is developed.

For a periodic system the permittivity tensor can be calculated as a sum over Lorentz oscillators, incorporating an imaginary loss component through the damping factor  $\sigma_k$ .<sup>16</sup> The frequencies of the oscillators are the transverse optic (TO) phonon frequencies of the system.

$$\bar{\epsilon}(v) = \bar{\epsilon}_{\infty} + \frac{4\pi}{V} \sum_k \frac{\bar{\mathbf{S}}_k}{v_k^2 - v^2 - i\sigma_k v} \quad \text{Equation 10a}$$

$$\bar{\mathbf{S}}_k = \bar{\mathbf{Z}}_k \bar{\mathbf{Z}}_k^T \quad \text{Equation 10b}$$

$$\bar{\mathbf{Z}}_k = \sum_a \bar{\mathbf{Z}}^a \bar{\mathbf{U}}_k^a \quad \text{Equation 10c}$$

$$\bar{\mathbf{D}} \bar{\mathbf{U}}_k = \Lambda_k \bar{\mathbf{U}}_k \quad \text{Equation 10d}$$

$$v_k^2 = \Lambda_k \quad \text{Equation 10e}$$

$V$  is the volume of the unit cell,  $\bar{\mathbf{S}}_k$  is the dipole oscillator strength tensor for the  $k^{\text{th}}$  transition, with a TO frequency of  $v_k$  and  $\bar{\boldsymbol{\epsilon}}_\infty$  the optical permittivity tensor, which represents the electronic contribution to the permittivity. The intensity of a transition,  $I_k$  is given by the trace of the oscillator strength tensor,  $I_k = \text{tr}(\bar{\mathbf{S}}_k)$ . The damping factor  $\sigma_k$  removes any discontinuities at the TO frequencies. Since the oscillator strengths and phonon frequencies can be calculated routinely in solid state quantum mechanical packages, the calculation of the frequency dependent complex permittivity using Equation 10a is straightforward. In some cases, using Equations 10b and 10c, PDielec calculates the oscillator strengths from the Born charge matrix for atom  $a$ ,  $\bar{\mathbf{Z}}^a$ , and the contribution of atom  $a$  to the  $k^{\text{th}}$  phonon mode,  $\bar{\mathbf{U}}_k^a$ .<sup>16</sup> As shown in Equation 10d, at the  $\Gamma$  point the  $k^{\text{th}}$  phonon mode is described by the eigenvector,  $\bar{\mathbf{U}}_k$ , and eigenvalue,  $\Lambda_k$ , of the mass weighted, dynamical matrix,  $\bar{\mathbf{D}}$ , which is a  $3N \times 3N$  matrix, where  $N$  is the number of atoms in the unit cell. The eigenvalues are the squared frequencies of the phonon modes (Equation 10e). The displacement of each atom in the  $k^{\text{th}}$  mode, is proportional to  $\bar{\mathbf{U}}_k^a / \sqrt{m_a}$ , where  $m_a$  is the mass of atom  $a$ . The dynamical matrix has  $3N$  eigenvectors and eigenvalues, of which three should be zero due to translational invariance. If there are any negative eigenvalues the system is unstable to some displacement and therefore not at an energy minimum.

For ionic systems it is common practice in solid state QM and MM programs to include a long wavelength, non-analytic correction to the mass weighted dynamical matrix at the  $\Gamma$  point, which describes the coupling of the longitudinal optic (LO) modes to the induced field resulting from the vibration. This may be written for atoms  $s$  and  $t$  and their Cartesian components  $\alpha$  and  $\beta$  as;<sup>16</sup>

$$(\bar{\mathbf{D}}_{\mathbf{q} \rightarrow 0}^{\text{LO}})_{s,\alpha;t,\beta} = (\bar{\mathbf{D}})_{s,\alpha;t,\beta} + \frac{4\pi}{V\sqrt{M_s M_t}} \frac{(\bar{\mathbf{q}}^T \bar{\mathbf{Z}}_s)_\alpha (\bar{\mathbf{q}}^T \bar{\mathbf{Z}}_t)_\beta}{\bar{\mathbf{q}}^T \cdot \bar{\boldsymbol{\epsilon}}_\infty \cdot \bar{\mathbf{q}}} \quad \text{Equation 11}$$

The mass weighting has been incorporated through the mass of the atoms,  $M_s$  and  $M_t$ . The correction depends upon the direction,  $\bar{\mathbf{q}}$ , that the long wave-length limit is approached. Diagonalisation of the corrected matrix gives the squared frequencies of  $N-1$  LO modes and  $2N-2$  TO modes (Equations 10d and 10e). In some of the examples given below the LO frequencies will be given for comparison with the TO frequencies.

## Effect of Particle Shape on Infrared Absorption

It has long been recognised that, especially for ionic materials, the local field within a crystal and its coupling with the transverse optic phonons has an important effect on the position and intensity of the absorption. Fröhlich<sup>17</sup> was one of the first to point out that the frequency of absorption of a

small ionic sphere embedded in a low dielectric medium is shifted to lie between the transverse and longitudinal optic frequencies of the material making up the sphere.

In the development of the theory used in PDielec an important assumption is that the particle size of the crystallites in the sample is small compared with the wavelength of light. Using this approach Genzel and Martin<sup>18</sup> were able to explain the observed infrared absorption of small spheres of MgO crystallites and the effect of the permittivity of the supporting medium on the spectrum. Studies of the infrared absorption by small particles of  $\alpha\text{-Fe}_2\text{O}_3$  using an effective medium theory and an absorption/scattering theory<sup>19,20</sup> showed that in order to fit the experimental spectra it was necessary to adjust not only the damping factors in Equation 10a, but also the permittivity of the matrix and the volume fraction of the dielectric medium. The latter was used to account for aggregation effects as the volume fraction increased. It was also shown that effective medium theories were only applicable for particles smaller than the wavelength of light. For larger particles the scattering from the particles becomes increasingly important.

More recently Balan and others in a series of papers<sup>20-24</sup> used density functional calculations together with an effective medium theory to calculate the infrared absorption of several minerals incorporating information about the crystallite shape. In an experimental and theoretical study of irradiated kaolinite<sup>24</sup> it was shown that exposure to radiation resulted in shifts in the infrared spectrum which could be accounted for by increasing the polarisability of the particles through an increase in the optical permittivity tensor.

The underlying theory adopted by PDielec is based on similar premises to the work described above, namely that the dielectric response of small spherical, ellipsoidal, slab-like or needle-like crystallites randomly distributed in a non-absorbing medium such as PTFE, KBr or Nujol, is the same as that of an effective medium material whose frequency dependent dielectric response can be calculated from the frequency dependent permittivity tensor of the crystal (as calculated by solid state QM or MM calculations), the shape of the crystallites and the permittivity of the non-absorbing medium (taken to be a constant over the frequency range of interest).

The development of the theory reported here closely follows the work of Sihvola<sup>25</sup>. It will be assumed that the inclusion particles, which may be non-isotropic, ellipsoidal (including spherical, needle-like and plate-like), are randomly orientated in an embedding, non-absorbing medium such as PTFE, KBr or Nujol. It should be emphasized that whilst PDielec can take account of particle shape, particle and matrix permittivity there are many additional aspects of infrared absorption which need to be considered when comparing calculated and experimental results. Most notable of these are; the coupling between phonons and mobile electrons or holes (so called phonon-polariton coupling)<sup>26</sup>, the scattering which starts to dominate as the particles get larger<sup>24</sup> and the agglomeration of particles as the volume fraction increases.

### **The polarisability of an isolated particle**

Figure 1 shows a schematic of the field and polarisation inside an inclusion with non-isotropic permittivity  $\bar{\epsilon}_i$  embedded in a supporting medium with permittivity  $\epsilon_e$ . The internal field within the inclusion is indicated by  $\bar{E}_i$ , the external, applied field is indicated by  $\bar{E}_e$  and the induced polarisation in the inclusion is shown by  $\bar{P}$ .

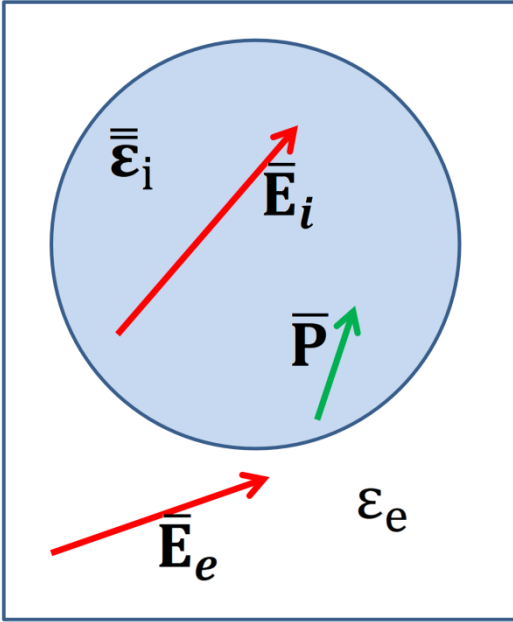


Figure 1: Schematic showing the field and polarisation inside an inclusion with non-isotropic permittivity  $\bar{\epsilon}_i$  embedded in a supporting medium with permittivity  $\epsilon_e$ . The internal field within the inclusion is indicated by  $\bar{E}_i$ , the external, applied field is indicated by  $\bar{E}_e$  and the induced polarisation in the inclusion is shown by  $\bar{P}$ .

The electric field internal to the inclusion gives rise to a polarisation density which is no longer necessarily aligned with the field because the material is non-isotropic. The polarisation density in the inclusion can be expressed as the tensor product of the permittivity contrast between the inclusion and the supporting medium and the (as yet unknown) internal field.

$$\bar{P} = (\bar{\epsilon}_i - \epsilon_e \bar{1}) \bar{E}_i \quad \text{Equation 12}$$

For any ellipsoidal shape (including sphere, slab and needle) with volume  $V$ , the polarisation density throughout the particle is uniform and integrating over all space gives the field induced dipole moment of the inclusion,  $\bar{p}$ .

$$\bar{p} = V \bar{P} = V(\bar{\epsilon}_i - \epsilon_e \bar{1}) \bar{E}_i \quad \text{Equation 13}$$

The dipole and the external field ( $\bar{E}_e$ ) are related by the polarisability tensor,  $\bar{\alpha}$ .

$$\bar{p} = \bar{\alpha} \bar{E}_e \quad \text{Equation 14}$$

Equations 13 and 14, allow the determination of the polarisability, once the field internal to the inclusion has been expressed in terms of the shape of the inclusion and its permittivity. The polarisation within the inclusion gives rise to a depolarisation field ( $\bar{E}_d$ ), which depends on the shape of the inclusion through the symmetric and unit trace depolarisation tensor,  $\bar{L}$ .

$$\bar{E}_d = -\frac{1}{\epsilon_e} \bar{L} \cdot \bar{P} \quad \text{Equation 15}$$

The internal field is the sum of the external field and the depolarisation field.

$$\bar{\mathbf{E}}_i = \bar{\mathbf{E}}_e + \bar{\mathbf{E}}_d$$

Equation 16

The depolarisation tensor acts as a projection or screening operator describing the effect of the geometry of the inclusion on the depolarisation field which results from its polarisation. For instance, in the case of a needle, only polarisation perpendicular to the needle axis contributes to the depolarizing field, whilst for a slab only polarization perpendicular to the slab face may contribute. Similarly for a sphere, all directions contribute and so the depolarisation matrix is diagonal with a value of 1/3 for each diagonal element, as the trace of the depolarisation tensor must be 1. It follows from Equations 12, 15 and 16 that;

$$\bar{\mathbf{E}}_i = \bar{\mathbf{E}}_e - \frac{1}{\varepsilon_e} \bar{\mathbf{L}} \cdot (\bar{\boldsymbol{\epsilon}}_i - \varepsilon_e \bar{\mathbf{1}}) \bar{\mathbf{E}}_i \quad \text{Equation 17}$$

Rearrangement allows the internal field of the inclusion to be expressed in terms of the known permittivities, the shape of the inclusion and the external field.

$$\begin{aligned} \bar{\mathbf{E}}_i (\varepsilon_e \bar{\mathbf{1}} + \bar{\mathbf{L}} \cdot (\bar{\boldsymbol{\epsilon}}_i - \varepsilon_e \bar{\mathbf{1}})) &= \varepsilon_e \bar{\mathbf{E}}_e \\ \bar{\mathbf{E}}_i &= \varepsilon_e \bar{\mathbf{E}}_e (\varepsilon_e \bar{\mathbf{1}} + \bar{\mathbf{L}} \cdot (\bar{\boldsymbol{\epsilon}}_i - \varepsilon_e \bar{\mathbf{1}}))^{-1} \end{aligned} \quad \text{Equation 18}$$

Substituting the internal field expression (Equation 17) into Equation 13 for the dipole moment and requiring the dipole moments calculated using the polarisation density to equal those calculated from the polarisability allows the polarisability to be written;

$$\bar{\alpha} = V \varepsilon_e (\bar{\boldsymbol{\epsilon}}_i - \varepsilon_e \bar{\mathbf{1}}) (\varepsilon_e \bar{\mathbf{1}} + \bar{\mathbf{L}} \cdot (\bar{\boldsymbol{\epsilon}}_i - \varepsilon_e \bar{\mathbf{1}}))^{-1} \quad \text{Equation 19}$$

Although it has not been specified explicitly the permittivity of the inclusion, and therefore the polarisability tensor, are frequency dependent through the oscillator strengths of each phonon mode contributing to the permittivity according to Equation 10a. The calculation of the complex, frequency dependent polarisability tensor of the composite material is the key step in the calculation of its effective permittivity.

### The Effective permittivity of a mixture

To extend this approach to include the effect of a number of inclusions we need to introduce the concept of an effective permittivity ( $\bar{\boldsymbol{\epsilon}}_{\text{ef}}$ ), which describes the behaviour of an average field,  $\langle \bar{\mathbf{E}} \rangle$ , where the angle brackets indicate an average over a volume of the composite material. It is required that the average electric flux density  $\langle \bar{\mathbf{D}} \rangle$  is the same in the effective medium as in the composite medium;

$$\langle \bar{\mathbf{D}} \rangle = \bar{\boldsymbol{\epsilon}}_{\text{ef}} \langle \mathbf{E} \rangle = \varepsilon_e \langle \bar{\mathbf{E}} \rangle + \langle \bar{\mathbf{P}} \rangle \quad \text{Equation 20}$$

The averaging is necessary because the polarisation within a given inclusion has an effect on the field in other inclusions. The local field in the cavity left by a single inclusion embedded in the average polarisation field is given by;

$$\bar{\mathbf{E}}_L = \langle \bar{\mathbf{E}} \rangle + \frac{1}{\epsilon_e} \bar{\mathbf{L}} \langle \bar{\mathbf{P}} \rangle$$
Equation 21

The local field ‘excites’ the inclusion resulting in a dipole moment  $\bar{\mathbf{p}}_{mi}^x$  that is related to the polarisation through the number density of inclusions ( $n$ ) and through the polarisability of the inclusion, which is already known from Equation 19.

$$\langle \bar{\mathbf{P}} \rangle = n \bar{\mathbf{p}}_{mi}^x = n \langle \bar{\alpha} \bar{\mathbf{E}}_L \rangle$$
Equation 22

The angle brackets around the product of the polarisability and the local field indicate that it is necessary to average the polarisation according to the distribution of alignments of inclusions. In this work it will be assumed that the inclusions are randomly aligned. Substituting the expression for the local field (Equation 21) gives;

$$\langle \bar{\mathbf{P}} \rangle = \left( \bar{\mathbf{1}} - \frac{n \langle \bar{\alpha} \bar{\mathbf{L}} \rangle}{\epsilon_e} \right)^{-1} n \langle \bar{\alpha} \rangle \langle \bar{\mathbf{E}} \rangle$$
Equation 23

## Mixing rules

There are many mixing rules which have been proposed to describe the homogenization of composite materials and a lot of work has been done in comparing their accuracy. Here two methods will be used. The first and the most commonly used method is the Maxwell-Garnett mixing rule.<sup>25</sup> Indeed this has been implied by the use of Equation 20 to define the effective permittivity. The other commonly used method is the Bruggeman mixing rule,<sup>25</sup> which differs substantially in the way the two components of the system are treated. It is usually stated that the Maxwell-Garnett mixing rule is good for low volume fractions of the inclusion and the Bruggeman approach should be better for higher volume fractions.<sup>27</sup> In addition to these mixing rules one other approach will be described, namely the Averaged Permittivity (AP) mixing rule, which calculates the absorption spectrum ignoring the effects of the internal field on the absorption and can therefore be used as an indicator of the shifts in frequency and intensity which have occurred owing to the effect of particle shape.

### Maxwell-Garnett mixing rule

The Maxwell-Garnett approach for treating the properties of heterogeneous mixtures assumes that the average field and the average flux density result from volume fraction weighted sums.

Substituting Equation 23 into Equation 20 gives the Maxwell-Garnett effective permittivity;

$$\bar{\epsilon}_{mg} = \bar{\mathbf{1}} + \left( \bar{\mathbf{1}} - \frac{n \langle \bar{\alpha} \bar{\mathbf{L}} \rangle}{\epsilon_e} \right)^{-1} n \langle \bar{\alpha} \rangle$$
Equation 24

The fact that the polarisability tensor has a volume term in it (Equation 19) means that the terms in Equation 24 containing  $n \bar{\alpha}$  depend on the volume fraction  $f$ . Although written as a tensor, because the assumption has been made that the inclusions are randomly orientated, the effective permittivity has to be diagonal with equal complex values. Since the polarisability is complex and

frequency dependent the effective permittivity is also and its calculation using Equations 24 and 19 needs to be calculated over the frequency range of interest.

### Bruggeman mixing rule

In the Maxwell-Garnett mixing formalism there is a distinction between the inclusion and the supporting medium which results in an asymmetry in the treatment of the two species in the mixture. Instead the Bruggeman mixing rule assumes that each species is polarized against the background of the effective medium and therefore the polarisation in the two components cancel each other out;

$$\langle \bar{\mathbf{P}}_1 \rangle + \langle \bar{\mathbf{P}}_2 \rangle = 0 \quad \text{Equation 25}$$

where the components are now labeled 1 and 2 rather than external and internal. The polarisation for species 1 and 2 with a number density of species represented by  $n_1$  and  $n_2$  can be obtained from the polarisability of the species (Equation 22);

$$\langle \bar{\mathbf{P}}_1 \rangle = n_1 \langle \bar{\alpha}_1 \rangle \bar{\mathbf{E}} \quad \text{Equation 26}$$

Substituting Equation 26 into Equation 25 leads to the requirement that;

$$n_1 \langle \bar{\alpha}_1 \rangle + n_2 \langle \bar{\alpha}_2 \rangle = 0 \quad \text{Equation 27}$$

Taking Equation 19 and generalizing it for species  $I$ , (where  $I$  is 1 or 2) embedded in an effective permittivity given by  $\bar{\epsilon}_{br}$ ;

$$\bar{\alpha}_i = V_i \bar{\epsilon}_{br} (\bar{\epsilon}_i - \bar{\epsilon}_{br}) \left( \bar{\epsilon}_{br} + \bar{\mathbf{L}} \cdot (\bar{\epsilon}_i - \bar{\epsilon}_{br}) \right)^{-1} \quad \text{Equation 28}$$

Equation 27 has to be solved for  $\bar{\epsilon}_{br}$ . Since the systems considered here are isotropic with random inclusions, a solution has to be found for a complex value of the Bruggeman permittivity at each frequency considered. An issue in the use of Equation 28 is that the same depolarisation matrix is being used for both species, which is clearly not always appropriate. The solution of Equation 27 can be achieved either by iteration or by casting the equation as a minimization problem. The iterative approach implemented in PDielec involves repeated application of Equation 29 until convergence.<sup>28</sup> The starting point for the iterations is taken as the Maxwell-Garnett solution for the first frequency and then the solution at the previous frequency is used to start the iterations.

$$\bar{\epsilon}_{br} = \frac{f_1 \bar{\epsilon}_1 [\bar{\mathbf{1}} + \bar{\mathbf{L}}(\bar{\epsilon}_1 - \bar{\epsilon}_{br})]^{-1} + f_2 \bar{\epsilon}_2 [\bar{\mathbf{1}} + \bar{\mathbf{L}}(\bar{\epsilon}_2 - \bar{\epsilon}_{br})]^{-1}}{f_1 [\bar{\mathbf{1}} + \bar{\mathbf{L}}(\bar{\epsilon}_1 - \bar{\epsilon}_{br})]^{-1} + f_2 [\bar{\mathbf{1}} + \bar{\mathbf{L}}(\bar{\epsilon}_2 - \bar{\epsilon}_{br})]^{-1}} \quad \text{Equation 29}$$

Although the Bruggeman permittivity is written here as a tensor, the polarisabilities in Equation 27 have to be averaged over the random orientation of the inclusions and therefore the homogenized material is isotropic with a single complex value for the diagonal tensor. Also, as with the Maxwell-Garnett mixing rule, since the polarisability is complex and frequency dependent, the effective

permittivity is also, and its calculation using Equation 29 needs to be performed over the frequency range of interest.

The choice between using the Bruggeman or Maxwell-Garnett model is often governed by the assumption that the Maxwell-Garnett model works well at low concentrations and the Bruggeman model works better at higher concentrations. Work by Karkkainen *et al.* using a finite difference method for random mixtures of non-absorbing materials indicated that the Bruggeman approximation works best when there is some clustering of the inclusions and the Maxwell Garnett model works best when there is no clustering.<sup>29</sup>

The Bruggeman solution has been shown to be unphysical in certain circumstances.<sup>30</sup> In particular when the real components of the permittivity have different signs and when the absolute values of the real components are much larger than those of the imaginary components. Unfortunately, it may be that these conditions will apply to modelling infrared absorption. As a result only a few of the examples discussed below will include results using the Bruggeman mixing rule; the majority will use the Maxwell-Garnett mixing rule.

### Averaged-Permittivity mixing rule

It is useful to be able to compare the effective medium theories with the absorption predicted using no shape information, that is using only the TO frequencies.

$$\bar{\epsilon}_{\text{TO}} = f\langle \bar{\epsilon}_i \rangle + (1 - f)\epsilon_e \quad \text{Equation 30}$$

Equation 30 defines an isotropic permittivity which can be used to calculate such an absorption coefficient. The angle brackets indicate an average of orientation. This mixing rule provides a useful comparison between the absorption calculated without any shape effects and that calculated including shape effects using the other mixing rules presented above. At low concentrations the peak positions of the AP mixing rule will be at the TO frequencies.

### Particle Size Effects

Meier and Wokaun<sup>31</sup> outlined an approach to treating large (metal) spherical particles, where particle size is incorporating terms up to 3<sup>rd</sup> order in the wave vector  $k$ . Using equations 12 and 16 we can write

$$\bar{\mathbf{P}} = (\bar{\epsilon}_i - \epsilon_e \bar{\mathbf{1}})(\bar{\mathbf{E}}_e + \bar{\mathbf{E}}_d) \quad \text{Equation 31}$$

$$\bar{\mathbf{E}}_d = -\frac{\left(1 - x^2 - i\frac{2}{3}x^3\right)}{\epsilon_e} \bar{\mathbf{L}} \cdot \bar{\mathbf{P}} \quad \text{Equation 32}$$

$$x = ak = \frac{2\pi a}{\lambda}$$

Here  $a$  is the size of the particle and  $x$  is the dimensionless ‘size’ of the particle with respect to the wavelength of the incident light. The first term relating the depolarisation field to the polarisability is the same as that used above in equation 15. The second term is a dynamic depolarisation term and the third term is a radiation damping correction to the electrostatic solution<sup>31</sup>.

A slightly different, but related, approach is presented by Sihvola<sup>25</sup>. Starting from Equation 17, a size dependent term  $G(x)$  is introduced as indicated by the work of Peltoniemi<sup>32</sup>;

$$\begin{aligned} G(x) &= G_1(x) + G_2(x) \\ G_1(x) &= \frac{2}{3}[(1+ix)e^{-ix} - 1] \\ G_2(x) &= \left(1+ix-\frac{7}{15}x^2-i\frac{2}{15}x^3\right)e^{-ix}-1 \end{aligned} \quad \text{Equation 33}$$

The modified equation for the relationship between the internal field and the external field based on equation 17 becomes;

$$\bar{\mathbf{E}}_i = \bar{\mathbf{E}}_e - \frac{(1-G(x))}{\epsilon_e} \bar{\mathbf{L}} \cdot (\bar{\boldsymbol{\epsilon}}_i - \epsilon_e \bar{\mathbf{1}}) \bar{\mathbf{E}}_i \quad \text{Equation 34}$$

This leads to a modified equation for the polarisability of spherical particles

$$\bar{\alpha}(x) = V \epsilon_e (\bar{\boldsymbol{\epsilon}}_i - \epsilon_e \bar{\mathbf{1}}) \left( \epsilon_e \bar{\mathbf{1}} + (1-G(x)) \bar{\mathbf{L}} \cdot (\bar{\boldsymbol{\epsilon}}_i - \epsilon_e \bar{\mathbf{1}}) \right)^{-1} \quad \text{Equation 35}$$

Using the modified, sized dependent polarisability all the Bruggeman and Maxwell mixing schemes can be implemented in a way that incorporates size effects.

Generally speaking the on-set of changes in the calculated absorption is an indication that size effects are important and should be treated properly.

## Light Scattering by Spherical Particles using Mie Theory

For particles which are comparable in size to the wavelength of light, the theory developed by Mie and described fully by van de Hulst<sup>14</sup> can be used. Unfortunately this theory is only applicable to spherical, isotropic particles where the separation between the particles is large compared with the wavelength of light.

PDielec implements a form of Mie theory using the Python library PyMieScatt<sup>33</sup>. In order to treat systems which are anisotropic, PDielec first of all transforms the real part of the permittivity so that the tensor is diagonal. Then the full permittivity (real and imaginary) is transformed to this basis.

$$\begin{aligned} \bar{\mathbf{U}}^T \bar{\boldsymbol{\epsilon}}_w^{\text{rea}} \bar{\mathbf{U}}^1 &= \bar{\boldsymbol{\epsilon}}^{\text{diag0}} \quad ^n \\ \bar{\boldsymbol{\epsilon}}^{\text{ne}} &= \bar{\mathbf{U}}^T \bar{\boldsymbol{\epsilon}}^{\text{ful}} \bar{\mathbf{U}}^1 \end{aligned} \quad \text{Equations 36}$$

The core of Mie theory is the calculation of efficiency factors  $S1(\theta)$  and  $S2(\theta)$  (page 125 in reference<sup>14</sup>). These factors depend upon the size of the particle with relative to the wavelength of the light ( $x$ ) and the refractive index of infrared active material ( $m_1$ ) relative to that of the supporting medium ( $m_2$ ). Both refractive indices are scalars,  $m_1$  is complex as light is absorbed by the material and  $m_2$  is assumed to be real.

For each of the three diagonal elements of  $\bar{\boldsymbol{\epsilon}}_{ne}^w$  the relative refractive index,  $m$  is calculated;

$$\begin{aligned}
m_1 &= \bar{\epsilon}_{w,w}^{\text{ne}} \\
m &= \frac{m_1}{m_2} \\
x &= \frac{2\pi a}{\lambda_c} \\
\lambda &= \frac{\lambda_{va}}{m_2}
\end{aligned}
\tag{Equations 37}$$

The size parameter depends upon the refractive index of the supporting medium because the wavelength of light is smaller than its vacuum value in a medium with a refractive index greater than one. The subscript  $w$  indicates one of the three directions  $x$ ,  $y$  or  $z$  in the basis which diagonalises the real permittivity tensor.

Using the routines available in PyMieScatt<sup>33</sup> the efficiency factor  $S(0)$  ( $S(0) = S_1(0) = S_2(0)$ ) is calculated from  $m$  and  $x$ . The extinction (this includes absorption and scattering) along with retardation are reflected in the overall complex refractive index (see page 129 in reference<sup>14</sup>);

$$\tilde{m}_w = m_2(1 - iS(0)2\pi Nk^{-3})$$

$$\begin{aligned}
N &= \frac{f_e}{V_{\text{spher}}} \\
V_{\text{spher}} &= \frac{4}{3}\pi a^3 \\
k &= \frac{2\pi}{\lambda}
\end{aligned}
\tag{Equations 38}$$

Here  $N$  is the number density of particles and  $k$  is the wave-vector of the light in the surrounding medium. The subscript  $w$  indicates that there are three values for the effective refractive index, depending on which diagonal value of the permittivity tensor is taken. Once the effective refractive index is known in each direction the effective permittivity can be calculated using the one third rule<sup>34</sup>;

$$\begin{aligned}
\tilde{m}_{ef}^f &= \frac{1}{3} \sum_w \tilde{m}_w \\
\varepsilon_{ef}^f &= \tilde{m}_{ef}^{2f}
\end{aligned}
\tag{Equations 38}$$

This approach to taking anisotropy into account when the embedded particles are anisotropic but randomly oriented is approximate, but has been shown to have a reasonably wide range of application.<sup>34</sup>

## IMPLEMENTATION

The above theory has been implemented in a Python 2/3 package which is available for download.<sup>35</sup> The package requires SCIPY<sup>36</sup>, NUMPY<sup>36</sup>, PyYAML<sup>37</sup> (py-yaml), PyMieScatt<sup>33</sup>, xlswriter<sup>38</sup> and if visualization of the predicted spectra is required MATPLOTLIB<sup>36</sup>. The program is run from the

command line. There are several command options and these are summarized below in Table 1. At the moment the package has interfaces to five solid state QM codes, VASP<sup>1</sup>, CASTEP<sup>2</sup> and CRYSTAL<sup>3</sup>, Abinit<sup>4</sup>, Quantum Espresso<sup>5</sup> and Phonopy<sup>6</sup>. In addition an interface is available for GULP<sup>5</sup> which is a force field based solid state code. The origin of the dataset(s) used for processing is determined by a command line switch, -program. An outline of the interfaces to these codes is given here. The package used for the calculation is described by the –program option. In addition a file name is given which contains the output which will be processed by PDielec.

**VASP** -program vasp OUTCAR

The name provided on the command line is an OUTCAR file. The OUTCAR is read by PDielec to determine the unit cell, atomic masses, frequencies, normal modes, born charge tensors and optical permittivity. The VASP run needs to be a DFPT calculation (IBRION=8).

**CASTEP** -program castep seedname

The name provided on the command line is the seedname for the calculation. The corresponding seedname.castep file in the current directory is read and processed to determine the unit cell, atomic masses, optical permittivity and born charge tensors. The normal modes and their frequencies are determined from the seedname.phonon file. The CASTEP run needs to be a DFPT (phonon+efield) task.

**CRYSTAL** -program crystal outputfilename

The name on the command line is a file ending in .out, containing the output of a CRYSTAL14 run. The contents of this file alone are sufficient to provide the unit cell, atomic masses, frequencies, normal modes and born charge tensors. However, the number of significant figures for the normal modes is not sufficient for an accurate calculation and it is therefore recommended that the HESSFREQ.DAT and BORN.DAT files are also made available. If they are present in the directory where PDielec is run from , it uses these files to calculate the born charge tensors, frequencies and normal modes. The CRYSTAL calculation needs to be a frequency calculation (FREQCALC) with the infrared intensity (INTENS) selected. The default algorithm does not calculate the optical permittivity, so this needs to be provided on the command line. However, if the CPHF or CPKS algorithm is used for the frequency calculation, the optical permittivity is calculated and PDielec will automatically read it from the output file. By default CRYSTAL projects out the pure translational modes of the system before calculating the frequencies, this can also done by the PDielec package. Small differences in the calculated frequencies between the CRYSTAL program and PDielec have been observed. These have been found to be due to a slightly different method for symmetrising the 2<sup>nd</sup> derivative matrix, because of this an optional directive “-hessian crystal” can be used to indicate that PDielec should use the same symmetrisation as Crystal14.

**ABINIT** -program abinit outputfilename

The output file should come from a run containing three datasets. One to calculate the wavefunction at the optimized geometry, one to calculate the field perturbations and one to calculate the second derivatives. Examples of input files and output files are available with the distribution.

**QE** -program qe outputfilename  
The output file is the dynamical matrix file, specified by “filedyn” in a run of the quantum espresso phonon package. Examples of input and output files are given in the PDIELEC distribution

**PHONOPY** -program phonopy vasp OUTCAR.born  
Phonopy calculates the dynamical matrix through numerical differentiation. It has interfaces to several programs, although PDIELEC has only used the VASP interface. In principle other interfaces could be used. The second parameter for the –program directive is the PHONOPY interface that was used to calculate the forces. Typically these would be generated by performing;

phonopy –d –dim="1 1 1"

to calculate the displacements in a set of POSCAR-\* files. After running VASP a single point VASP calculation for each displacement. The FORCE\_SETS file can then be calculated using for example;

phonopy –f DISP-\*/vasprun.xml

where the DISP-\* directories are where the VASP calculation was performed. Finally a dynamical is written out using;

phonopy –dim="1 1 1" –qpoints="0 0 0" –writedm

To calculate the infrared spectrum PDIELEC needs the Born charges for the atoms in the unit cell and these can be calculated using VASP and the optimized geometry of the unit cell. The OUTCAR file from this calculation can be copied to the current directory and is renamed OUTCAR.born

**GULP** -program gulp outputfilename  
The name on the command line is a file ending in .gout, containing the output of a GULP run. The contents of this file alone are sufficient to provide the unit cell, atomic masses, frequencies, normal modes, born charge tensors and optical permittivity. Because GULP only writes out the born charge matrices for the asymmetric unit, it is necessary to run a frequency calculation using P1 symmetry and a complete unit cell. The key words; nosymm, phonon, intensity, eigen and cart are recommended for the GULP calculation. In the case that no shells are used in the calculation the optical permittivity is not available in the output and it is necessary to provide it on the command line (see –optical and –optical\_tensor options below).

**EXPERIMENT** -program experiment filename

This option has been added to allow the exploration of ‘toy’ problems. The file contains a minimum amount of data to allow a calculation to proceed. It is assumed that the systems will be isotropic as that make the input simpler. Calculations of the LO frequencies will not work with this option. An example input file is given here, which gives results very similar to that found for the Castep, MgO example;

```
species 2      # Define the atomic species, followed by the number of species
O 16.0        # Species name followed by its mass
Mg 24.3
```

```

lattice 2.12346 # Define the lattice, the parameter is a scaling factor
1 1 0          # The a vector
1 0 1          # The b vector
0 1 1          # The c vector
unitcell 2      # Define the unit cell contents and fractional coordinates
O  0.5 0.5 0.5 # Species fraca, fracb, fracc
Mg 0.0 0.0 0.0 # Species fraca, fracb, fracc
static          # Define the static permittivity
3.13969 0.0   0.0
0.0  3.13969 0.0
0.0  0.0   3.13969
frequencies 3    # Specify how many frequencies to read in
388.282 0.000073639 # The frequency in wavenumbers and oscillator strength
388.282 0.000073639
388.282 0.000073639

```

Examples of data sets for these packages are included with the distribution. The interface to these QM and MM codes reads information about the unit cell, the calculated normal modes and the Born charge matrices; from these the permittivity is calculated over the frequency range requested. The absorption and molar absorption coefficients can be plotted along with the real and imaginary permittivities. Optionally all the information can be written to a comma separated values (csv) file for direct importing into a spreadsheet. The program is run from the command line. There are several command options and these are summarized below in Table 1. Some of the options may be repeated. The package needs a shape to be specified (sphere, needle, plate or ellipse). If no shape is specified on the command line a sphere is assumed.

Table 1: PDielec command line options

Option	Default	Purpose	R <sup>a</sup>
-program string		string can be “abinit”, “castep”, “crystal”, “gulp”, “qe”, “experiment” or “vasp” and specifies the program which generated the results to be analysed	
-method string	maxwell	The method is given by the string and is either ‘ap’, ‘maxwell’, ‘bruggeman’ or ‘mie’	✓
-sphere		The inclusion is a sphere, the default if no other shape is given.	
-needle h k l		The inclusion is a needle whose unique direction is given by the direction [hkl].	✓
-plate h k l		The inclusion is a plate whose surface is defined by the Miller indices (hkl). Note that needles and ellipsoid use directions in crystal coordinates defined by [hkl]. For non-orthogonal lattices the normal to the (hkl) is not necessarily the same as [hkl].	✓
-ellipse h k l z		The inclusion is an ellipsoid, whose unique direction is given by [hkl], z specifies the eccentricity of the ellipsoid.	✓
-vf real	0.1	real specifies the volume fraction	✓
-mf real	0.0	real specifies a mass fraction from which the volume fraction is calculated. The calculation requires the density of the supporting matrix.	✓
-matrix string	ptfe	The supporting matrix is defined by the string. Options are “ptfe”, “kbr”, “17ujol”, “air”, “vacuum”, “ldpe”, “mdpe”, “hdpe”. If the matrix is given in this way both the density and the permittivity of the supporting matrix are defined. Alternatively the density and dielectric options can be used.	
-density real	2.2	real defines the density of the supporting matrix	
-dielectric real	2.0	real defines the dielectric of the supporting matrix	
-LO h k l		The frequencies corresponding to the longitudinal optic modes with a k vector direction (h k l) are calculated using Equations 10 and 11	✓
-LO_cart x y z		As above but for Cartesian directions	✓
-sigma real	5.0	real specifies the damping factor, $\sigma$ , for all modes in $\text{cm}^{-1}$ , as used in Equation 10a	
-mode_sigma k z		The k'th mode is assigned a specific $\sigma$ ( $\text{cm}^{-1}$ ) given by z.	✓
-vmin real	0.0	real is the starting wavenumber ( $\text{cm}^{-1}$ ) for the frequency range	
-vmax real	300.0	real is the final wavenumber ( $\text{cm}^{-1}$ ) for the frequency range	
-l real	0.2	real is the increment used to cover the frequency range ( $\text{cm}^{-1}$ )	
-plot sstring		Plot types are specified by the string and they can be ‘absorption’, ‘molar_absorption’, ‘real’ or ‘imaginary’	✓
-excel s		Writes the results to an excel spread sheet with the name specified by the string s.	
-csv s		Output is sent to a comma separated file specified by the string s.	

-csv_ext string		Output is sent to 3 comma separated files; string_command.csv, string_frequency.csv and string_spectrum.csv	
-print		Additional output is provided from the QM or MM calculation	
-ignore k		Ignore the kth mode (any mode less than 5cm <sup>-1</sup> is ignored automatically)	✓
-mode k		Only use the kth mode in the calculation of the permittivity	✓
-threshold z1 z2		The modes selected for inclusion in the absorption calculation have to have an IR intensity greater than z1 and a frequency greater than z2. By default z1 and z2 are 1.0e-10 and 5cm-1 respectively.	
-eckart		The translational modes are projected out of the hessian before diagonalisation	
-hessian string		string may be either “crystal” or “symm”. In the case of “crystal” the hessian is symmetrised using the same algorithm as Crystal14. “symm” is the default	
-optical z1 z2 z3		z1,z2 and z3 define the diagonal of the optical permittivity tensor	
-optical_tensor z1 z2 ..z9		z1,..9 define the full optical permittivity tensor	
-masses string		string can be either “program”, “average” or “isotopic”, meaning that the masses used in the calculation of the frequencies are either taken from the QM program or are the average of the isotope abundances or are the most abundant isotope mass.	
-mass string real		The atomic mass of string is set to real. This can be used to explore the effect of isotope substitution on the calculated frequencies.	✓
-processors int		The number of processors to be used in the calculation can be defined. By default all available processors are used.	
-molesof string [int]		By default string is “cells”. Other options are “atoms” or “molecules”. If ‘molecules’ is specified then the number of atoms in a molecules must be provided	
-size real [sigma]		Used to modified polarisability (Eq. 34) for spherical particles which incorporates the radius of the particle in microns(real).  It is also used to specify the dimension of the spherical particles for the Mie method.  It is also possible to specify a size distribution in which case the first number is the mean of the log distribution (in microns) and the second is its width (in log(microns)).	✓

<sup>a</sup>This column indicates if a command line option can be used more than once.

The shape options; ellipse, slab and needle, specify a unique axis [hkl] using the crystal axes of the unit cell. PDielec transforms these to a cartesian coordinate system using the unit cell lattice vectors. In the case of a slab morphology the unique direction is normal to the surface specified by its Miller indices (hkl). The definitions of the various depolarisation tensors are indicated in Table 2 below.

Table 2: Definitions used of the depolarisation tensor

Sphere	$\bar{\mathbf{L}} = \frac{1}{3}(\bar{\mathbf{V}}_1\bar{\mathbf{V}}_1^T + \bar{\mathbf{V}}_2\bar{\mathbf{V}}_2^T + \bar{\mathbf{V}}_3\bar{\mathbf{V}}_3^T)$
Slab	$\bar{\mathbf{L}} = \bar{\mathbf{V}}_1\bar{\mathbf{V}}_1^T$
Needle	$\bar{\mathbf{L}} = \frac{1}{2}(\bar{\mathbf{V}}_2\bar{\mathbf{V}}_2^T + \bar{\mathbf{V}}_3\bar{\mathbf{V}}_3^T)$
Ellipsoid	$\bar{\mathbf{L}} = a\bar{\mathbf{V}}_1\bar{\mathbf{V}}_1^T + b\bar{\mathbf{V}}_2\bar{\mathbf{V}}_2^T + b\bar{\mathbf{V}}_3\bar{\mathbf{V}}_3^T$

d

The three directions defined by  $\bar{\mathbf{V}}_1$ ,  $\bar{\mathbf{V}}_2$  and  $\bar{\mathbf{V}}_3$  are mutually orthogonal cartesian vectors calculated from [hkl] for an ellipse, slab or needle or (hkl) for a slab. In the case of a slab, needle or ellipsoid,  $\bar{\mathbf{V}}_1$  defines the unique direction and the other vectors are orthogonal to it. For the case of an ellipsoid, the parameters  $a$  and  $b$  in Table 2 depend on the ratio, z, of the length of unique axis length over the length of an axis perpendicular to it.<sup>25</sup>

$$\text{For } z > 1 \text{ the ellipsoid is prolate } e = \sqrt{1 - z^{-2}}, a = \frac{(1-e^2)}{2e^3} \left( \ln \frac{1+e}{1-e} - 2e \right), b = \frac{1}{2}(1-a)$$

$$\text{For } z < 1 \text{ the ellipsoid is oblate } e = \sqrt{z^{-2} - 1}, a = \frac{(1+e^2)}{e^3} (e - \tan^{-1} e), b = \frac{1}{2}(1-a)$$

From an experimental point of view it is often convenient to use a mass fraction rather than a volume fraction to indicate the amount of dielectrically active material present. PDielec allows mass fractions to be specified instead of a volume fraction, but this requires that the density of the supporting matrix is known. For convenience the package has a small database of the common supporting materials shown in Table 3 below. These can be specified through the -matrix option. In the case that the properties of the support material are different the properties can be defined instead with the -dielectric and -density options.

Table 3: Physical properties of matrix materials in PDielec

Name	Density	Permittivity	Description
ptfe	2.2	2.0	polytetrafluoroethylene
air	0.0	1.0	air
vacuum	0.0	1.0	vacuum
kbr	2.75	2.25	potassium bromide
nujol	0.838	2.155	Nujol
hdpe	0.955	2.25	high density polyethylene
mdpe	0.933	2.25	medium density polyethylene
ldpe	0.925	2.25	low density polyethylene

The optical permittivity is normally calculated by the QM or MM program concerned. However, as this property reflects the electronic contribution to the permittivity at zero frequency, unless there is some treatment of electrons by the shell model, then in MM calculations the optical permittivity needs to be defined through the command line options -optical or -optical\_tensor.

Unlike the other methods ‘mie’ method cannot work with particles of zero radius. All methods therefore use a default size of 1.0E-12 microns. The Mie approach is only valid for dilute dispersions and for spherical particles. However, if other shapes are specified the Mie method will still be called and the results will be applicable to spheres of the specified size.

## Parallelization, threads and performance

To improve the performance of the program python parallelization has been used to parallelize over the frequencies, shapes and methods. By default this parallelization spawns additional Python executables, depending on the number of cores available.

In addition to this form of parallelization the NUMPY library can use multi-threaded BLAS. NUMPY can be compiled with several different BLAS libraries, including; MKL (from Intel), OPENBLAS and ATLAS, or indeed no optimized BLAS library is necessary. To explore the BLAS version compiled with your version of NUMPY please use the test\_numpy\_1, test\_numpy\_2 and test\_numpy\_3 scripts included in the Python/ subdirectory. If you are using MKL or OPENBLAS, the number of threads being used needs to be set with the MKL\_NUM\_THREADS or OPENBLAS\_NUM\_THREADS environment variable (sometimes OMP\_NUM\_THREADS is also used). Use the test routines to determine the optimum for your system. Experience indicates that no performance benefit is obtained with more than two threads. In the case of Phonopy the dynamical matrix is read from a yaml file. This has been found to be very slow unless the C parser is used. If the C parser is not available a warning is issued and the program reverts back to the Python parser.

Finally the use of non-standard BLAS libraries seems to cause problems with the affinity settings for the multiprocessing. It has been noticed that the parallel processes can all end up executing on the same processor. In order to prevent this, before executing the pdielec and preader scripts it may be necessary to include;

```
export OPENBLAS_MAIN_FREE=1
```

For some reason this also works if the MKL library is being used.

## Example command line uses of PDIELEC

```
pdielec -method ap -method maxwell -sphere -plate 0 0 1 -needle 0 0 1 -LO 0 0 1 .
```

This performs a calculation using the Averaged-Permittivity and Maxwell-Garnett mixing rules for spherical particles, plate-like particles with a surface (001) and needle-like particles with a unique direction lying along the [001] direction. The supporting matrix is taken to be PTFE and the default volume fraction (10%) is used. The results of a VASP calculation are stored in the current directory. There is no absorption output from this command as neither the -plot nor the -csv options were specified. The output includes the calculation of the LO modes along the (001) direction.

```
pdielec -vmin 300 -vmax 800 -sphere -dielectric 3 -vf 0.1 -vf 0.2  
-sigma 10 -csv mgo.csv phonon
```

This performs a calculation for spherical particles varying the frequency from 300 to 800 cm<sup>-1</sup>, the permittivity of the supporting media is 3, two volume fractions are considered and a damping factor of 10 cm<sup>-1</sup> is used. The results of a CASTEP calculation with the seed-name “phonon” are analysed

and the results stored in mgo.csv for further analysis using a spreadsheet. In this example a Maxwell-Garnett mixing rule is used by default.

If visual inspection of the results is required then

```
pdielec -vmin 300 -vmax 800 -sphere -dielectric 3 -vf 0.1 -vf 0.2  
-sigma 10 -csv mgo.csv -plot molar_absorption phonon
```

will perform the same calculation but a graph showing the molar absorption coefficients will be displayed.

```
pdielec -matrix hdpe -method ap -method maxwell -sphere -plate -1 -1 -2 \  
-vmax 2000 -mf 0.1 calcite.gout -csv calcite.csv
```

This command performs a calculation of the absorption spectrum resulting from a GULP calculation. The supporting matrix density and permittivity are those of high density polyethylene, the frequency range is 0 to 2000 cm<sup>-1</sup>, the mass fraction considered is 10%, the mixing rules used are Averaged-Permittivity and Maxwell-Garnett. Spheres and plates with the (112) surface are considered.

```
pdielec -method mie -sphere -mf 0.1 -program vasp OUTCAR -size 0.1 -size 1.0 -size 1.0 -csv results.csv
```

This command performs a calculation of the absorption spectrum resulting from a VASP calculation using the Mie method for sphere with several particles sizes.

```
pdielec -sphere -mf 0.1 -program experiment experiment.expt -size 0.1 -size 1.0 -size 1.0 -csv results.csv
```

This command performs a calculation of the absorption spectrum resulting from the data stored in the experiment.expt file. Maxwell-Garnett calculations are performed with 3 different sized spheres and the results stored in a csv file.

## Contents of the csv output file

If a csv output file is requested the file will contain the command used to perform the calculation. A brief summary is given of each active infrared mode; including the mode number, frequency, intensity, integrated molar absorption coefficient, its peak height (calculated from the intensity and damping factor) and the damping parameter used in the calculation. Following this is a table with a column for frequency followed by columns containing the real and imaginary permittivities, the absorption and molar absorption coefficients at each frequency.

## Parallelization

PDielec has been written to make use of multiprocessor computers. On a 4 processor machine the speed-up is nearly linear up to 4 processors, as can be seen in the Figure below.

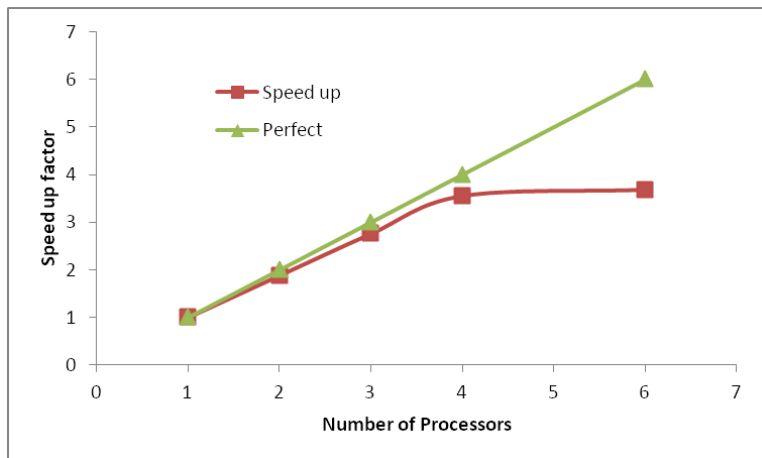


Figure 2: Speed up on a 4 processor machine

## EXAMPLES

Several examples are given to illustrate applications of the package. The calculations used to provide the data for the permittivities are sufficiently accurate to illustrate aspects of the theory. The examples are chosen to show the package being used with the QM packages CASTEP and VASP and with the MM package GULP.

### MgO using CASTEP

Magnesium oxide is an isotropic medium, the initial unit cell and the space group symmetry ( $Fm\bar{3}m$ ) were taken from the Inorganic Crystal Structure Database (ICSD)<sup>39</sup> reference number ICSD-52026.<sup>40</sup> The primitive cell was optimized using CASTEP. Norm-conserving pseudo-potentials were used to represent the core electrons of magnesium and oxygen. An energy cutoff of 1000 eV was used with the PBE<sup>41</sup> density functional and a k-point spacing for the Monkhorst-Pack grid of  $0.04 \text{ \AA}^{-1}$ . The primitive cell was optimized and a Density Functional Perturbation Theory (DFPT) calculation of the phonon spectrum at the gamma point was performed. The optimised lattice parameter was found to be  $2.1234 \text{ \AA}$ , compared with the experimental value of  $2.107 \text{ \AA}$ . Only 3 degenerate modes contribute to the permittivity. A summary of the results is presented in Table 4.

Table 4: Calculated Properties of MgO

Property	Values(s)		Units
Unit cell dimensions <sup>a</sup>	2.123 (2.107)		Å
Space group	<i>Fm</i> $\bar{3}$ <i>m</i>		
Optical permittivity	3.14		
Static permittivity	10.0		
Phonon frequency (intensity) <sup>b</sup>	TO T 388.3 (9.29)	LO (001) 693.7	cm <sup>-1</sup> (D/Å) <sup>2</sup> /amu

<sup>a</sup>The experimental value is given in brackets

<sup>b</sup>The intensities are given in brackets, T indicates a triply degenerate mode

Because MgO is isotropic with only a single frequency contributing to the permittivity, it makes a useful example application to illustrate several features of PDIELEC. The real and imaginary frequency dependent permittivities are shown in Figure 3, where a damping factor ( $\sigma$ ) of  $10\text{ cm}^{-1}$  has been used. In the Figure the real permittivity at zero frequency corresponds to the static permittivity in Table 4, and at frequencies above the absorption at  $388\text{ cm}^{-1}$  the permittivity tends to the optical permittivity as the frequency increases. The real permittivity has zero values at  $388.3\text{ cm}^{-1}$  and  $693.7\text{ cm}^{-1}$  which are the TO and LO frequencies respectively.

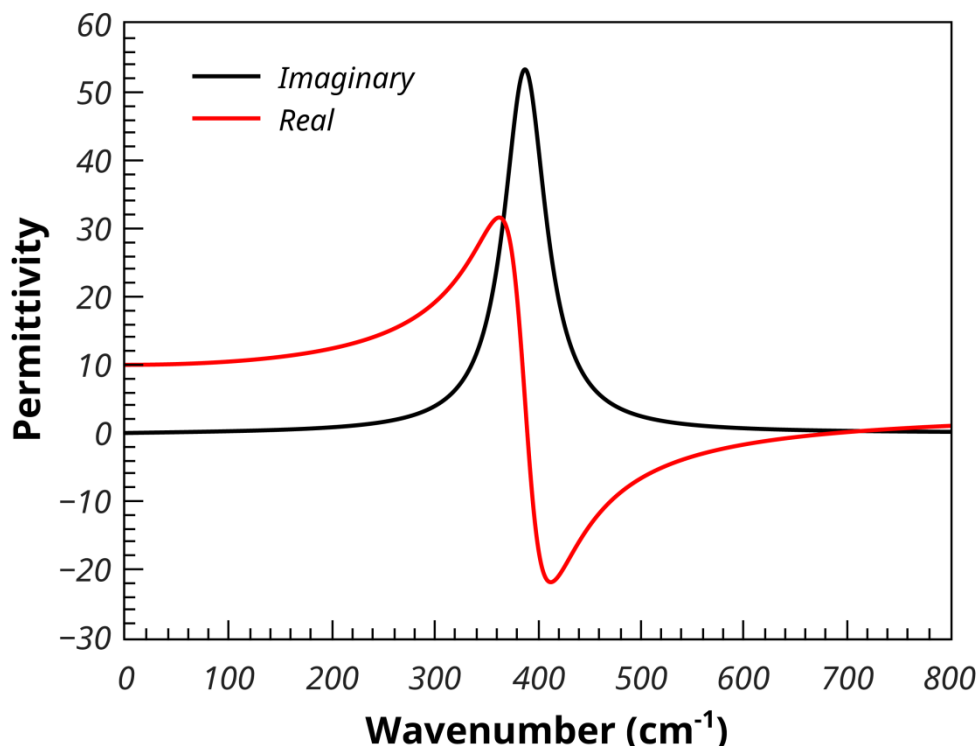


Figure 3: Permittivity of MgO

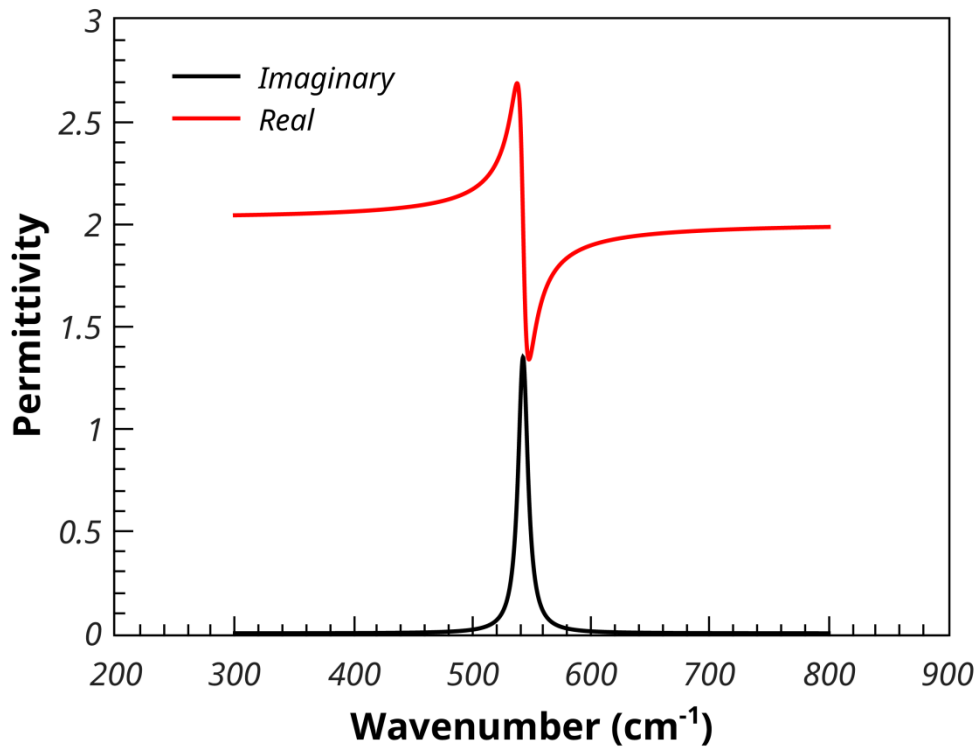


Figure 4: Real and Imaginary permittivities of a 10% volume fraction of MgO spheres in PTFE, calculated using the Maxwell-Garnett method

Using the Maxwell-Garnett mixing rule, Figure 4 shows the calculated permittivities of a 10% volume fraction of MgO spheres in a supporting medium with a frequency independent permittivity of 2.0, which would be typical of a material such as PTFE. Due to the dilution effect the real component has shifted to a base line value close to 2, and the absorption, as indicated by the maximum in the imaginary component has shifted by about  $150\text{ cm}^{-1}$  to  $550\text{ cm}^{-1}$ .

The effect of volume fraction on the predicted molar absorption coefficient, using the Maxwell-Garnett mixing rule, is shown in Figure 5. The lowest volume fraction of MgO gives the largest shift of the absorption peak to high frequency. As the volume fraction increases the mixing rule predicts a broadening of the absorption, whilst the peak in the molar absorption coefficient moves to lower frequency. At the highest loading ( $f=0.9$ ) the maximum absorption occurs quite close to the TO frequency. The Maxwell-Garnett mixing rule is regarded as being appropriate for low volume fractions and so should not be used for interpreting results in which higher volume fractions of absorbing media have been used.<sup>25</sup>

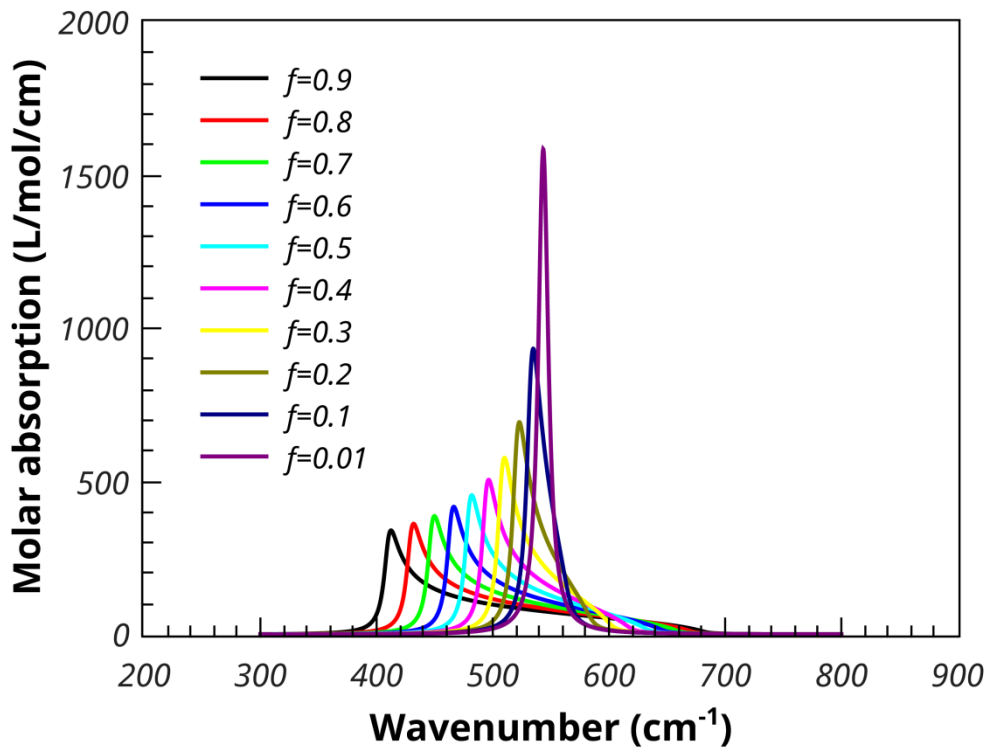


Figure 5: Effect of volume fraction on the Maxwell-Garnett molar absorption coefficient of MgO spheres in PTFE

Figure 6 shows the same plot for the Bruggeman mixing rule. At low volume fractions the Bruggeman mixing rule predicts a similar absorption to the Maxwell-Garnett. Indeed as the volume fraction approaches zero the two rules predict the same absorption characteristics. However, even at the relatively low 1% loading , the Bruggeman mixing rule shows additional broadening of the peak, the shape of the absorption peak has lost its Lorentzian characteristic shape as can be seen clearly in Figure 5 At 10% loading the Bruggeman predicted absorption is broad with the peak shifted to lower wavenumber. This broadening increases with increased loading until, at the higher loadings, the TO peak begins to dominate the absorption.

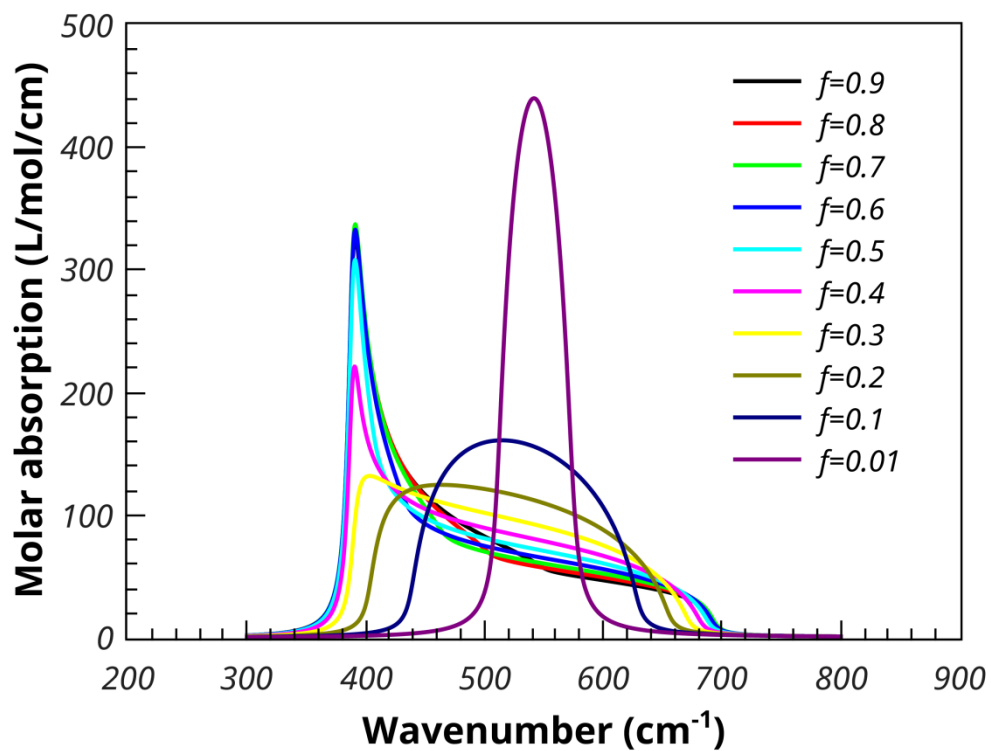


Figure 6: Effect of volume fraction on the Bruggeman molar absorption coefficient of MgO spheres in PTFE

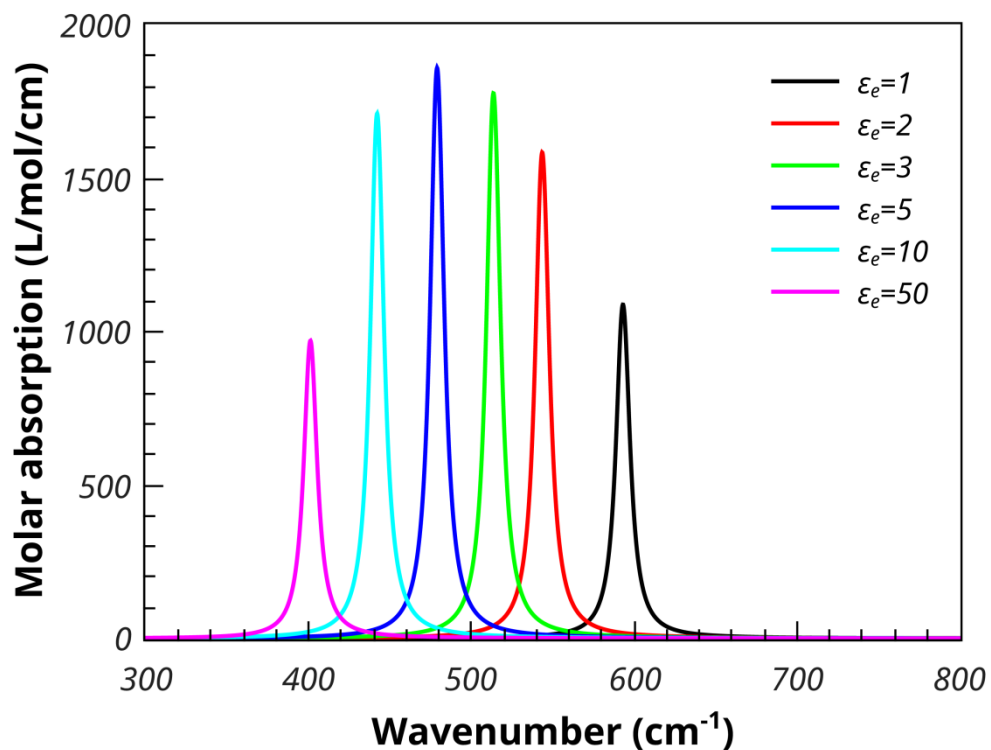


Figure 7: The Maxwell-Garnett molar absorption coefficients of spherical MgO particles, 1% volume fraction, embedded in media of varying permittivities

Figure 7 shows the effect of varying the permittivity of the supporting medium. The calculations were performed on spherical MgO particles with a 1% volume fraction. The lowest permittivity is that of a vacuum (or air) and shows the highest shift of the absorption maximum to higher frequencies. Increasing the permittivity lowers the shift until it becomes quite small. A similar effect is seen for the Bruggeman mixing model. However, the absorption resulting for particles in a low dielectric medium is considerable broader than that seen in the Maxwell-Garnet case. This broadening reduces as the permittivity of the medium increases (see Figure 8).

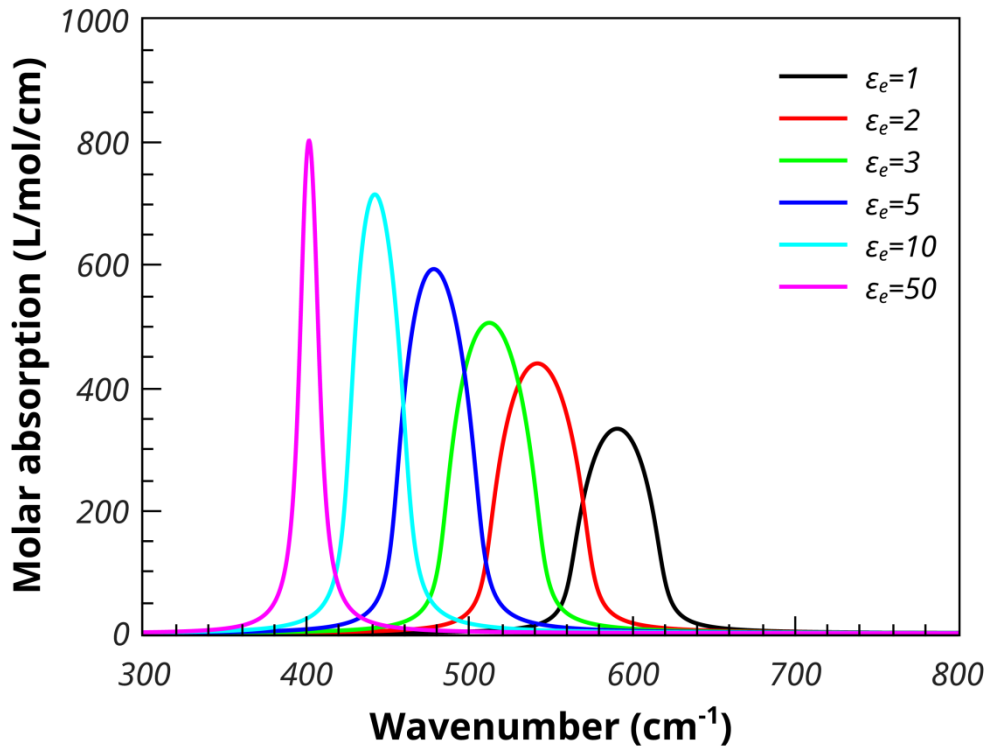


Figure 8: The Bruggeman molar absorption coefficients of spherical MgO particles, 1% volume fraction, embedded in media of varying permittivities

### ZnO using VASP

Zinc oxide crystallizes in space group P6<sub>3</sub>mc (wurtzite). All calculations were performed by VASP<sup>1</sup> using projector augmented-wave PAW<sup>42</sup> pseudo-potentials, the PBE<sup>41</sup> density functional, an energy cutoff of 600 eV and a k-point resolution of approximately 0.1 Å<sup>-1</sup>. The initial unit cell was taken from the ICSD<sup>39</sup> with code ICSD-26170.<sup>43</sup> The unit cell and atom positions were optimized using VASP and the permittivity was calculated using DFPT and the results reported in Table 5. Only two of the bands showed any significant intensity, a doubly degenerate band (E) with a TO frequency of 372.1 cm<sup>-1</sup> and a non-degenerate band (A) with a TO frequency of 350.0 cm<sup>-1</sup>. The LO frequency of the non-degenerate band is shifted to 502.0 cm<sup>-1</sup> for a wave-vector with direction (001), whilst the degenerate modes are unaffected. In the case of the (010) direction the LO frequency of one of the E modes is shifted to 511.2 cm<sup>-1</sup>. It is known that ZnO can crystallize with a plate morphology<sup>44</sup> with the (001) surface dominant. Calculations of the molar absorption were performed for a sphere,

plate and needle like shapes with the unique directions of the plate and the needle being normal to the (001) surface. A volume fraction of 1% was chosen for these calculations and the predicted molar absorption coefficients for the Maxwell-Garnett mixing rule is shown in Figure 9.

Table 5: Calculated properties of ZnO

Property	Values(s)			Units
Unit cell dimensions <sup>a</sup>	$a,b = 3.295(3.25)$ $c = 5.285(5.207)$			Å
Space group	P6 <sub>3</sub> mc			
Optical permittivity <sup>b</sup>	5.09, 5.09, 6.0			
Static permittivity <sup>b</sup>	10.83, 10.83, 11.67			
Phonon frequency (intensity) <sup>c</sup>	TO A 350.0 (17.1) E 372.1 (16.4)	LO (001) 502.0	LO (010) 511.2	$\text{cm}^{-1} (\text{D}/\text{\AA})^2/\text{amu}$

<sup>a</sup>The experimental values are given in brackets

<sup>b</sup>Only the diagonal components are given

<sup>c</sup>The intensities are given in brackets, E and A indicate a doubly and non- degenerate mode respectively

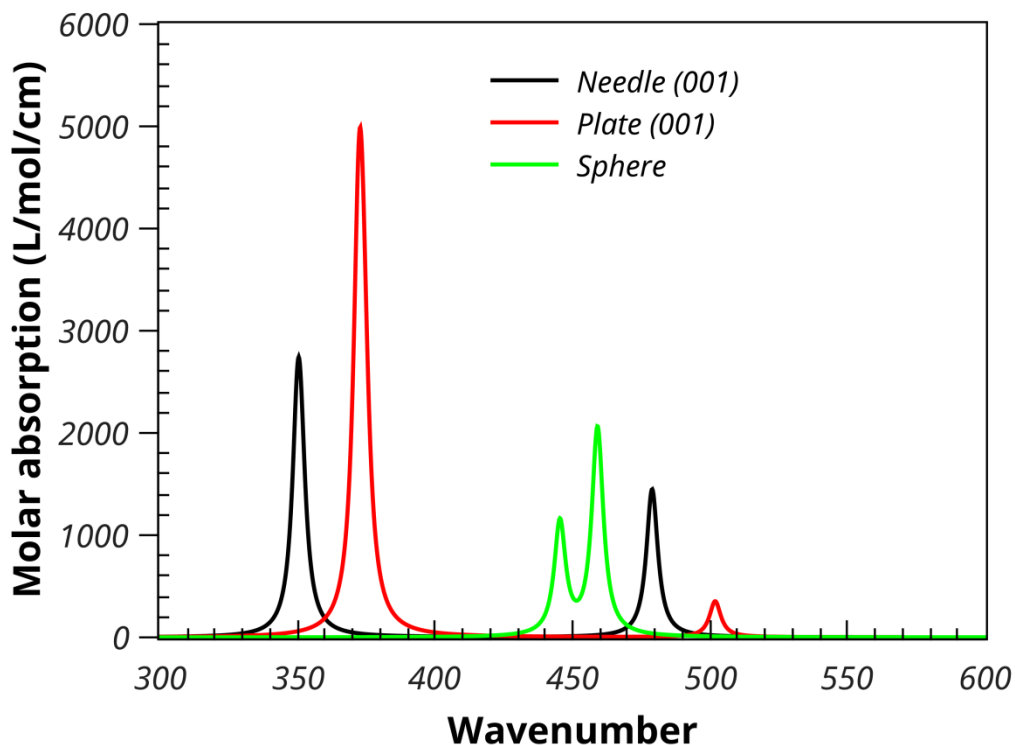


Figure 9: The effect of shape on the Maxwell-Garnett molar absorption coefficient of 1% volume fraction ZnO in PTFE

For the Maxwell-Garnett mixing rule the sphere morphology results in the two absorption peaks shifting from their TO positions to higher wavenumber by about  $80 \text{ cm}^{-1}$ . The plate morphology

results in one of the peaks moving to higher wavenumber by about  $130\text{ cm}^{-1}$ , whilst the other remains at the TO position. The Maxwell-Garnett results are in close accord with some experimental results by Yamamoto et al.<sup>45</sup> who measured the infrared spectrum of ZnO smoke particles and observed peaks in the absorption at  $380, 530$  and  $550\text{ cm}^{-1}$ . Previous work<sup>46,47</sup> has also used effective medium theory to explain the observed spectrum.

## Calcite using GULP

Calcite is the most stable polymorph of calcium carbonate and the crystal structure belongs to the  $R\bar{3}c$  space group. The force field and atomic structures used here are described in detail in work by Fisler *et al.*<sup>48</sup> Briefly, the oxygen ions are described using a core-shell model.<sup>49</sup> The carbon - oxygen potential of the carbonate is taken to be a Morse potential and an additional 3 atom potential is used to maintain the O-C-O angle at  $120^\circ$ . The van der Waals interactions between non bonded atoms are taken to be Buckingham potentials and the charges on the calcium, carbon and oxygen ions are +2, +1.3435 and -1.1145 respectively. The shell charge of the oxygen ion is -2.133 and the spring constant for the core-shell interaction is  $52.74\text{ eV}/\text{\AA}^2$ .

The unit cell was optimized using the primitive unit cell and the full space group symmetry. The calculation of the phonon spectrum was performed without symmetry but still using the primitive cell of the lattice. A summary of the calculated properties is given in Table 6.

Table 6: Calculated properties of calcite

Property	Values(s)	Units
Primitive cell dimensions <sup>a</sup>	$a,b,c = 6.376$ (6.375) $\alpha,\beta,\gamma = 46.0$ (46.1)	$\text{\AA}$ degrees
Space group	$R\bar{3}c$	
Optical permittivity <sup>b</sup>	1.91, 1.91, 2.0	
Static permittivity <sup>b</sup>	6.7, 6.7, 7.1	
Phonon frequency (intensity) <sup>c</sup>	TO E 114.8 (2.39) A 127.4 (3.36) A 249.3 (1.23) E 320.7 (5.82) A 338.1 (4.14) E 620.1 (3.38) A 732.0 (26.89) E 1463.6 (16.97)	$\text{cm}^{-1}$ ( $D/\text{\AA}$ ) <sup>2</sup> /amu

<sup>a</sup>The experimental values taken from reference<sup>48</sup> are given in brackets

<sup>b</sup>Only the diagonal components are given

<sup>c</sup>The intensities are given in brackets, A and E indicate a non- and doubly- degenerate mode respectively.

Figure 10 shows the results of analysis of the results using PDielec. The damping parameter used in the calculation was a value of  $5\text{ cm}^{-1}$ . A 10% volume fraction was used with sphere and plate morphologies for the particles. The unique axis for the plate was taken to be the normal to the (211) surfaces in the primitive cell axes (or the {104} surfaces in the standard unit cell). Such surfaces define the rhombohedral faces commonly seen in calcite crystals.<sup>50</sup> Figure 10 shows that the doubly degenerate TO absorption peak at  $620\text{ cm}^{-1}$  is not significantly affected by spherical particles and there is a small shift to higher frequencies in the case of plate-like particles. The non-degenerate TO transition at  $732\text{ cm}^{-1}$ , which corresponds to motion of the carbon atom of the carbonate along the unique direction of the slab, shows a shift to  $786$  and  $819\text{ cm}^{-1}$  for the sphere and plate respectively. The doubly degenerate peak at  $1463\text{ cm}^{-1}$  is shifted to  $1480\text{ cm}^{-1}$  by spherical particles and is split by plate-like particles with one component which shifts to  $1491\text{ cm}^{-1}$ .

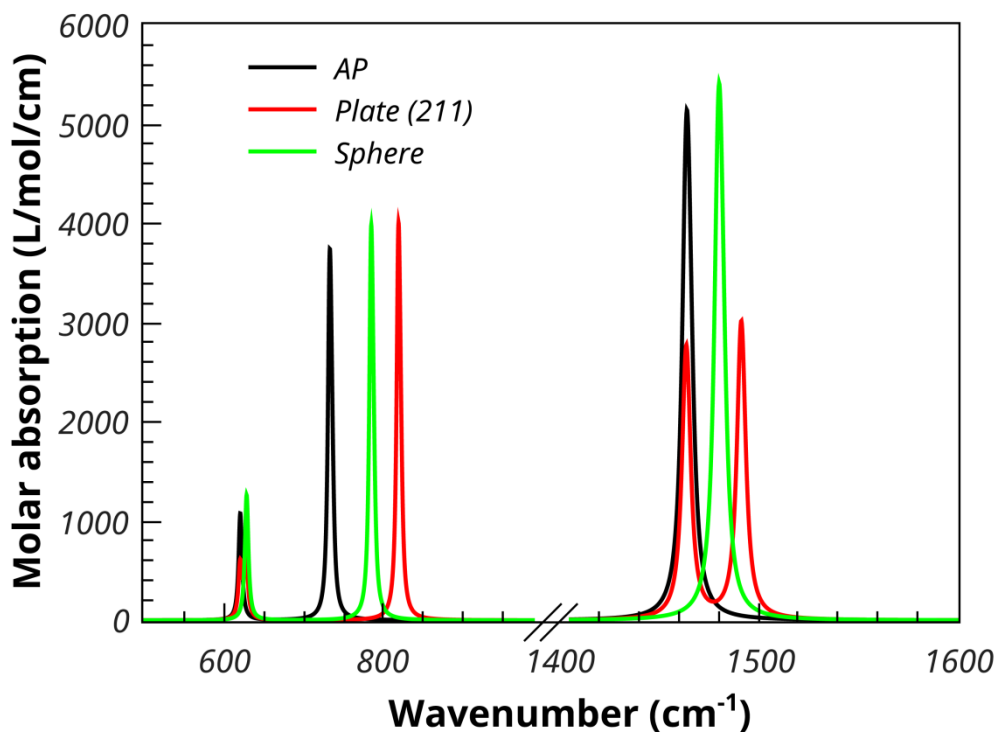


Figure 10: Calculated Maxwell-Garnett absorption spectrum of 10% volume fraction of calcite in PTFE

### Fluoroapatite using VASP

The line shapes of the infrared absorption of apatite and fluoroapatite were examined extensively by Balan *et al.*<sup>22</sup> Their calculations included the effect of crystallite habit on the spectrum and the results reported here are similar to their conclusions. The method used by Balan *et al.* is an infinitely dilute Maxwell-Garnett model, so the only difference between the methods used by them and those reported here using PDielec are the incorporation of the volume fraction into the theory and the use of an ellipsoidal shape for comparison with the other shapes.

All calculations were performed by VASP<sup>1</sup> using projector augmented-wave PAW<sup>42</sup> pseudo-potentials, the PBE<sup>41</sup> density functional, an energy cutoff of 600 eV and a k-point resolution of approximately 0.1 Å<sup>-1</sup>. Table 7 summarises the results of the calculations. Only the 3 highest frequency bands are reported and discussed. The TO intensity of the highest frequency band at 1038 cm<sup>-1</sup> is low and will not be discussed further. The Bravais Friedel Donnay Harker (BFDH)<sup>51</sup> crystal habit of the optimized crystal is shown in Figure 11. The habit was calculated using the Mercury software package.<sup>52</sup> The BFDH crystal habit is often used to give an idea of the likely important faces of a crystal. It uses only the crystal lattice and space group to determine the crystal morphology. Figure 11 shows that the {100} surfaces form a tube which are capped by the {011} surfaces. The effect of different particle shapes on the predicted spectrum is shown in Figure 12. The calculations of the spectra were performed with a damping parameter ( $\sigma$ ) of 2 cm<sup>-1</sup>. The ellipsoid was chosen to have an aspect ratio, a/b, of 2 and a principle axis along [001], which was compatible with the morphology predicted by the BDFH method. The two TO absorption frequencies at 981 and 986 cm<sup>-1</sup> have A and E symmetry respectively. Spherical crystallites result in three absorption peaks at around 1000, 1010 and 1015 cm<sup>-1</sup>. Needle shaped crystallites leave the A symmetry TO absorption peak at 981 cm<sup>-1</sup> unaffected, but shift and split the E symmetry TO peak to 1020 and 1046 cm<sup>-1</sup>. A plate morphology with (100) surfaces results in the A and one component of the E TO absorption peak remaining at the TO frequencies, with the other component of the E shifting 85 cm<sup>-1</sup> to 1075 cm<sup>-1</sup>. The ellipsoidal morphology show three shifted peaks at 1000, 1018 and 1045 cm<sup>-1</sup>. These results are consistent with those of Balan *et al.*<sup>22</sup>, who gave detailed results for hydroxyapatite.

Table 7: Calculated properties of fluoroapatite

Property	Values(s)	Units
Primitive cell dimensions <sup>a</sup>	a,b = 9.447, c = 6.926 (9.417, 6.875)	Å
Space group	P6 <sub>3</sub> m	
Optical permittivity <sup>b</sup>	2.891, 2.891, 2.894	
Static permittivity <sup>b</sup>	12.081, 12.081, 8.841	
Phonon frequency (intensity) <sup>c</sup>	TO A 981.8 (112.6) E 986.3 (101.0) E 1038.1 (7.92)	cm <sup>-1</sup> (D/Å) <sup>2</sup> /amu

<sup>a</sup>The experimental values taken from Hughes *et al.*<sup>53</sup> are given in brackets

<sup>b</sup>Only the diagonal components are given

<sup>c</sup>The intensities are given in brackets, E and A indicate doubly and non- degenerate modes respectively

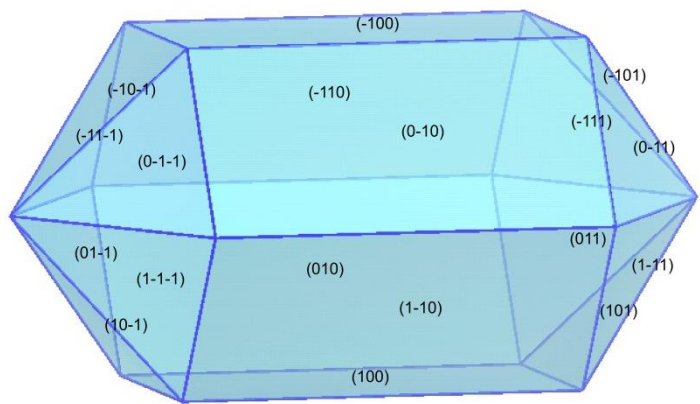


Figure 11: BDFH Morphology of fluoroapatite

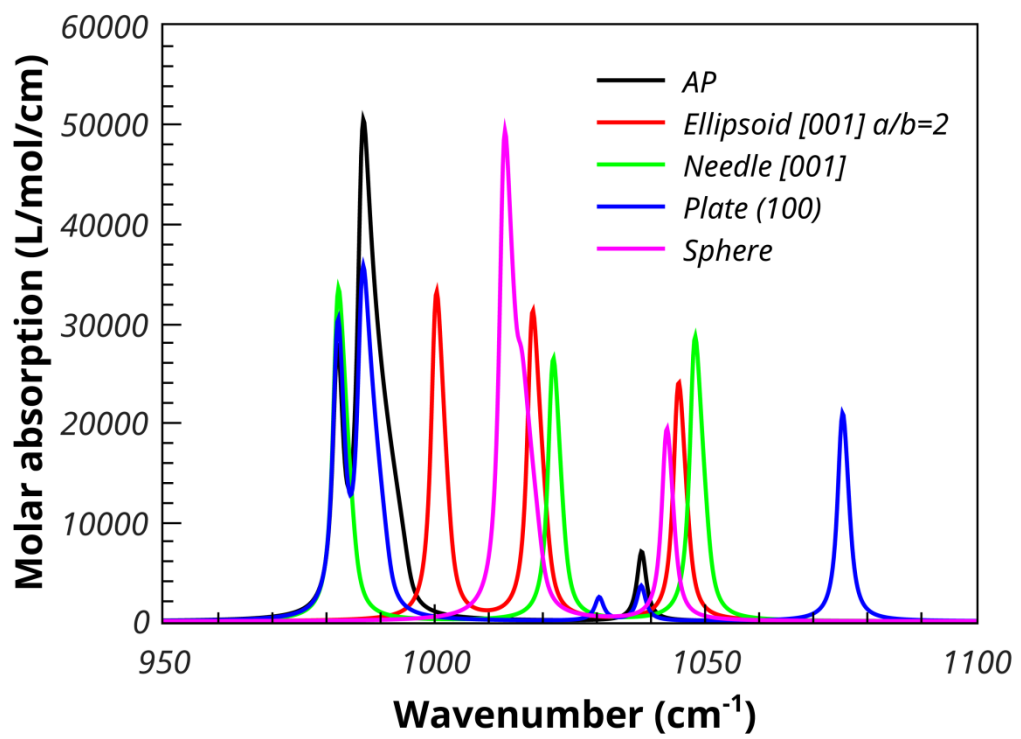


Figure 12: Calculated Maxwell-Garnett absorption spectra of 10% fluoroapatite in PTFE

## L-aspartic Acid using CASTEP

L-aspartic acid is a zwitterion in the solid state and so the shape of the particles used in the measurement of IR and THz spectra maybe important. The starting geometry for optimization of the unit cell and molecular structure of L-aspartic acid was taken from Derissen et al.<sup>54</sup> The PBE<sup>41</sup> functional was used with a plane wave energy cutoff of 1000 eV and norm conserving pseudo-potentials. A dispersion correction using the Tkatchenko-Scheffler scheme<sup>55</sup> available in CASTEP was applied for both the geometry optimisation and the calculation of the phonon spectrum at the gamma point, with a value  $S_6$  scaling factor<sup>55</sup> of 1.0. A summary of the results of the calculations is shown in Table 8.

Table 8: Calculated properties of L-aspartic Acid

Property	Values(s)	Units
Unit cell dimensions <sup>a</sup>	$a = 7.597$ (7.617) $b = 7.028$ (6.982) $c = 5.113$ (5.142) $\beta = 98.77$ (99.84)	Å
Space group	$P2_1$	
Optical permittivity <sup>b</sup>	2.68, 2.20, 2.56	
Static permittivity <sup>b</sup>	4.58, 3.65, 3.65	
Phonon frequency (intensity) <sup>c</sup>	TO 84.5 (0.120) 104.7 (0.202) 106.0 (0.243) 115.3 (0.474) 137.3 (0.617) 1290.0 (55.0) 2945.9 (102.8) 2947.3 (48.2) 3053.7 (44.1)	$\text{cm}^{-1}$ ( $\text{D}/\text{\AA}$ ) <sup>2</sup> /amu

<sup>a</sup>The experimental values are taken from Derissen et al.<sup>54</sup> are given in brackets

<sup>b</sup>Only the diagonal components are given

<sup>c</sup>Only selected transitions are tabulated. The intensities are given in brackets.

The THz spectrum of L-aspartic acid has been reported by Juliano and Korter<sup>56</sup> in the frequency range 0-90  $\text{cm}^{-1}$ . The infrared spectrum has been reported and assigned by Lopez et al.<sup>57</sup> Figure 13 shows the calculated absorption spectra for L-aspartic acid for three frequency ranges. The

calculation of the spectra used the Maxwell-Garnett mixing rule with a 10% volume fraction of L-aspartic acid in PTFE and for comparison the TO mixing rule. A damping factor of  $2\text{ cm}^{-1}$  was used. Spherical and a variety of plate-like inclusions were used to illustrate their effect on the absorption spectra. Figure 13a shows the frequency range from  $60$ - $130\text{ cm}^{-1}$  which is that covered by THz spectroscopy. The shifts observed for the different particle morphologies are not large, but the change in intensities is significant. The molecular motions associated with phonons at these frequencies tend to be whole molecule motion involving rotation. Figure 13b shows the frequency range from  $1260$ - $1340\text{ cm}^{-1}$ . In this frequency range bending of the carboxylate anion contributes to the spectrum significantly. The three different plate morphologies show different and significant shifts in the TO absorption peak at  $1290\text{ cm}^{-1}$ . The spherical morphology shows a shift of around  $25\text{ cm}^{-1}$  to higher wavenumber. Figure 13c shows the spectra in the frequency range  $2900$ - $3100\text{ cm}^{-1}$ , which corresponds to the motion of O-H (below  $2980\text{ cm}^{-1}$ ) and N-H (above  $2980\text{ cm}^{-1}$ ) stretching. The effect of the different possible crystal morphologies is large with shifts to higher frequency of up to  $50\text{ cm}^{-1}$ . The spectra below  $3000\text{ cm}^{-1}$  arises from two TO absorptions at  $2946$  and  $2947\text{ cm}^{-1}$ . Because the motions associated with each mode interact differently with the internal field within each crystal they give rise to different shifts producing more complex spectra.

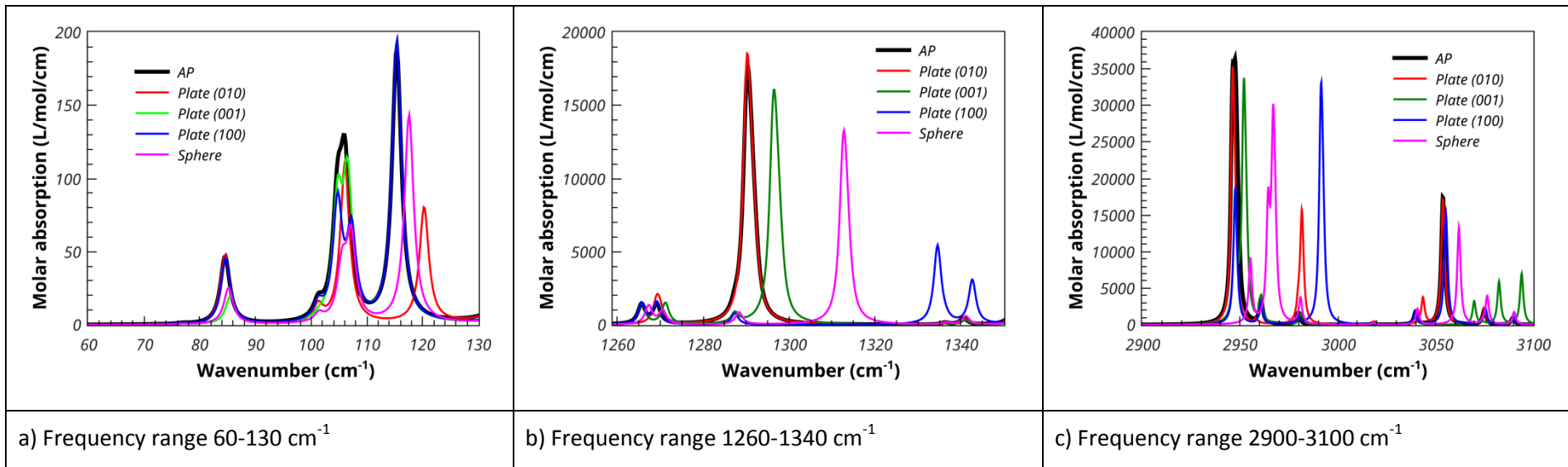


Figure 12: Calculated Maxwell-Garnett absorption spectra of 10% volume fraction of L-aspartic acid in PTFE

## MgO Example using Mie Scattering

Figure 13 compares a Mie scattering calculation with the results from Maxwell-Garnett effective medium theory. The same data set was used for the CASTEP, MgO example. A volume fraction of 1% was used with a small sphere radius ( $0.1 \mu$ ) and a broadening of  $5 \text{ cm}^{-1}$  embedded in a matrix of PTFE. A power expansion in the size parameter of the Mie expressions indicates that for small sizes of particles, the Mie and the Maxwell-Garnett methods should be the same. This is verified in Figure 13.

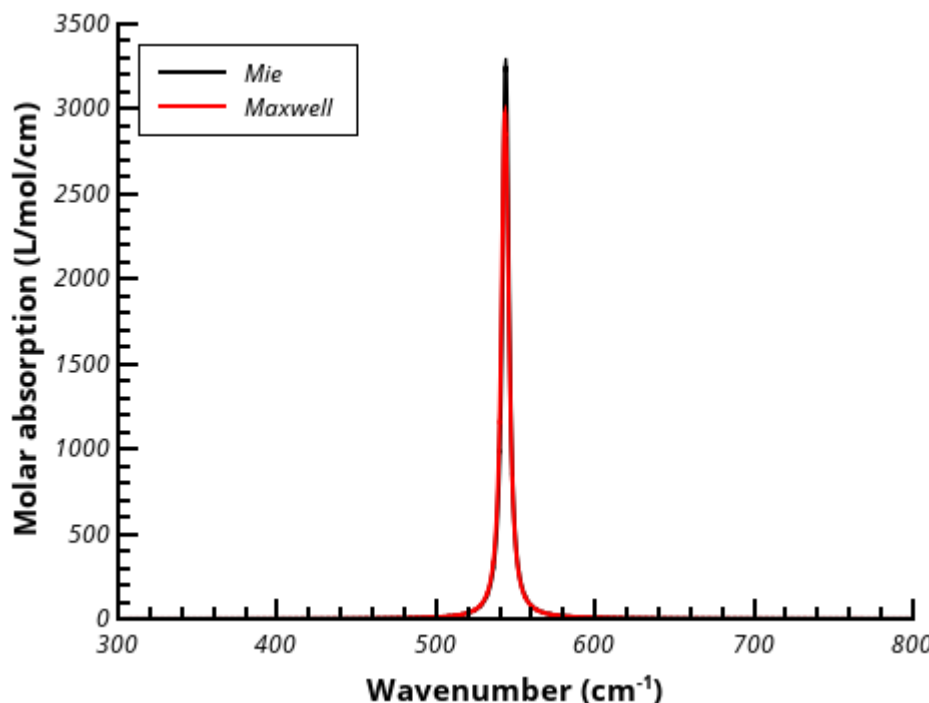


Figure 13: Comparison of Mie and Maxwell methods. 1% volume fraction of MgO in PTFE, sphere radius of  $0.1 \mu$  and a broadening of  $5 \text{ cm}^{-1}$

To better understand what makes particles large or small Table 9 shows the dimensionless size parameter,  $x$ , as a function of wavenumber and of sphere radius (equations 37) . It has been assumed that the supporting medium is PTFE. Since the power expansion of the size parameters leads to terms which are quadratic in  $x$ , it should be expected that when  $x$  is less than about 0.1, the particles can be considered small. It can be seen that particles less than  $0.01\mu$  are small over the range of frequencies considered. But while  $0.1\mu$  particles are small in the THz regime and low frequency infrared they should not be considered small over the more extended infrared frequencies.  $1\mu$  particles should be considered large for both the THz and the extended infrared.

Figure 14 shows how the Mie predictions change as the particle radius changes from  $0.2$  to  $1.6\mu$ . As the particle size increases the peak above  $500 \text{ cm}^{-1}$  splits into two. One broader peak which moves to lower frequency as the particle size increases and the peak at about  $550 \text{ cm}^{-1}$  which loses intensity as the particle size increases. There is also the onset of absorption at  $388 \text{ cm}^{-1}$  which corresponds to the bulk TO modes.

Table 9: Variation of size parameter with wavenumber and radius of sphere

Wavenumber (cm <sup>-1</sup> )	Radius of sphere (μ)				
	0.001	0.01	0.1	1	10
100	0.0009	0.0089	0.0888	0.8884	8.8841
200	0.0018	0.0178	0.1777	1.7768	17.7682
300	0.0027	0.0267	0.2665	2.6652	26.6523
400	0.0036	0.0355	0.3554	3.5536	35.5364
500	0.0044	0.0444	0.4442	4.4420	44.4204
600	0.0053	0.0533	0.5330	5.3305	53.3045
700	0.0062	0.0622	0.6219	6.2189	62.1886
800	0.0071	0.0711	0.7107	7.1073	71.0727
900	0.0080	0.0800	0.7996	7.9957	79.9568
1000	0.0089	0.0888	0.8884	8.8841	88.8409

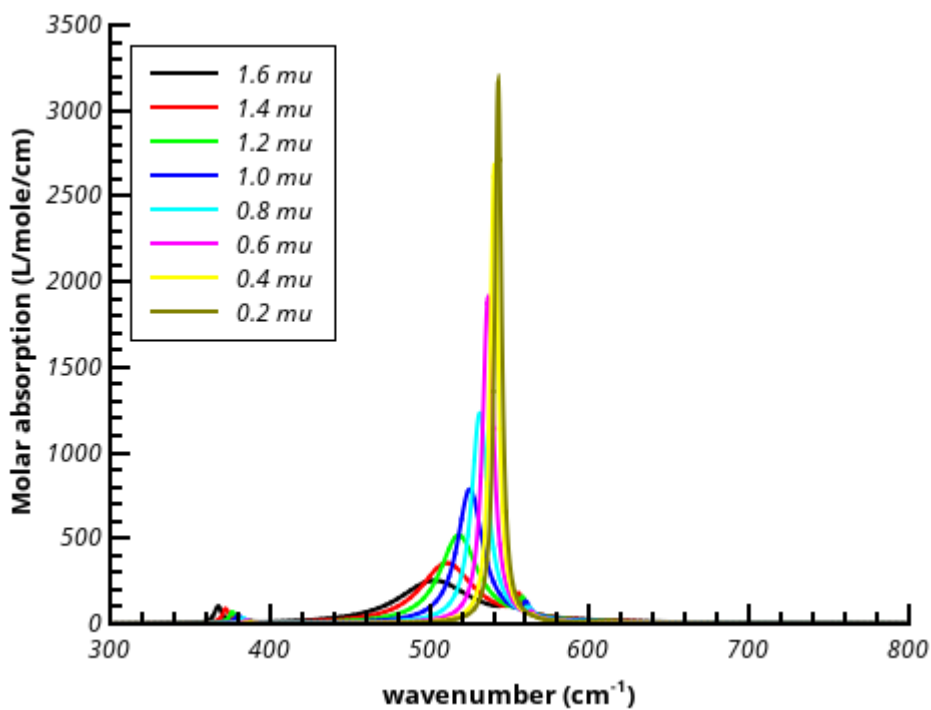


Figure 14: Variation in absorption calculated by the Mie method for different radii of spheres. 1% volume fraction of MgO in PTFE and a broadening of 5 cm<sup>-1</sup>

Figure 15 shows the effect of increasing the particle size further. More structure appears in the absorption, with increasing absorption around the bulk TO frequency. Above 4.0μ there is more low frequency structure appearing, below 300cm<sup>-1</sup>.

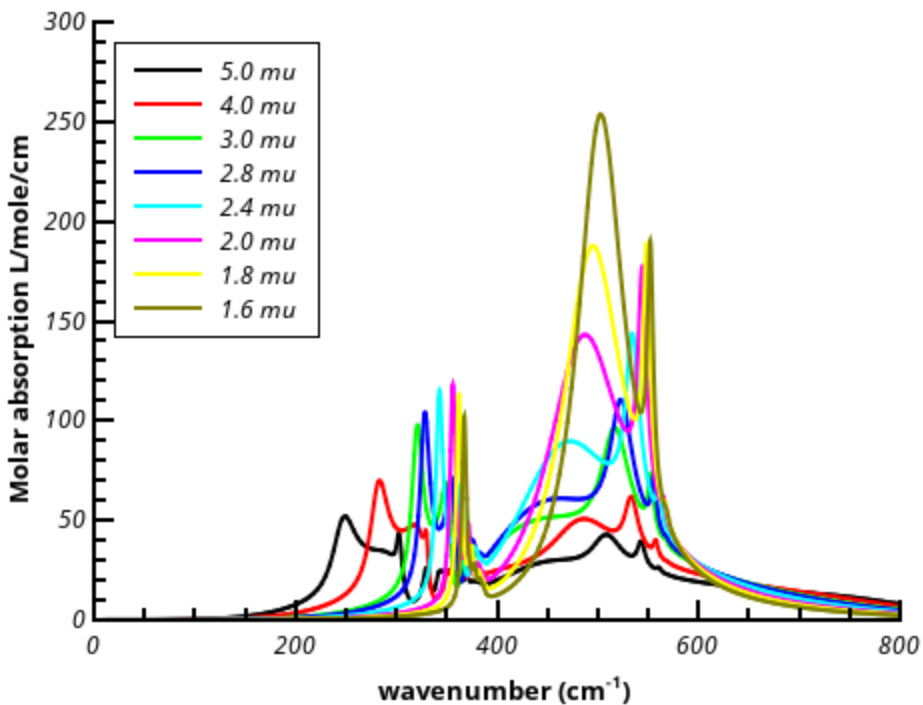


Figure 15: Variation in absorption calculated by the Mie method for different radii of spheres. 1% volume fraction of MgO in PTFE and a broadening of  $5\text{ cm}^{-1}$

### ZnO Example using Mie Scattering

ZnO is an anisotropic material, so the treatment described here using Mie scattering is an approximation. However, the permittivity constant tensor is diagonal due to the space group symmetry of the crystal. Figure 16 compares the predicted absorption using Mie and Maxwell-Garnett for different volume fractions of  $0.1\mu\text{m}$  ZnO spheres embedded in PTFE. A line broadening of  $5\text{ cm}^{-1}$  was assumed.

Figures 16 and 17 compare the capabilities of the Maxwell-Garnett and Mie methods for describing volume fraction effects. Figure 16 shows that Maxwell-Garnett predicts a lowering of intensity and frequency of the high frequency peak as the volume fraction is increased. Figure 17 shows that Mie theory shows no effect of the change in volume fraction. This is to be expected as the theory assumes that each sphere is isolated and not affecting the other spheres around it. It should be pointed out that the figures are plotting molar absorption coefficients. The actual absorption would increase with volume fraction of ZnO (see equation 2).

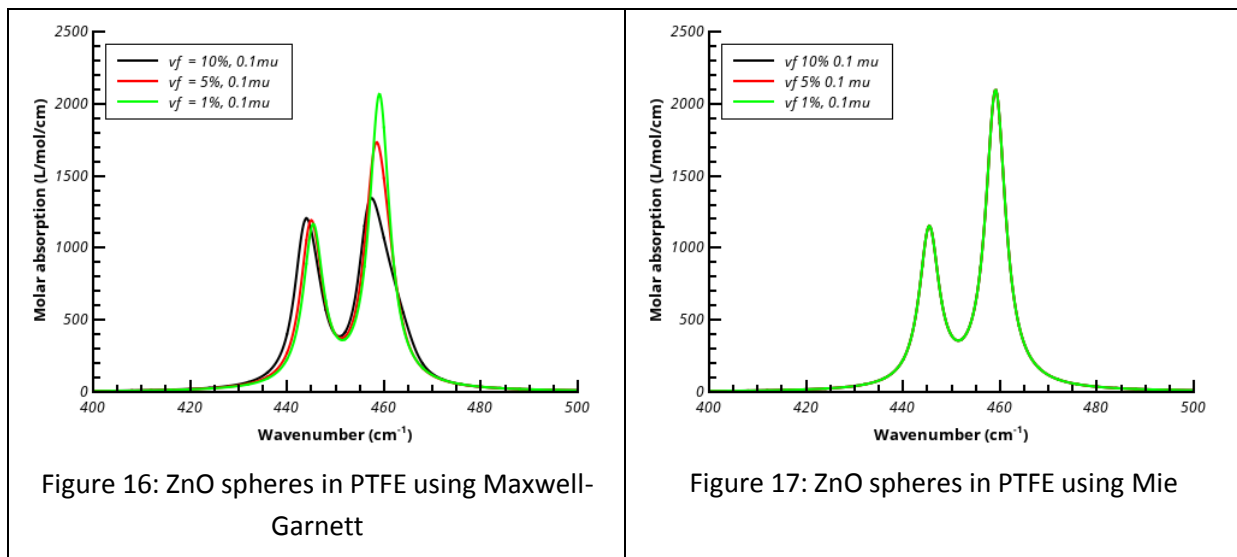


Figure 18 shows that the variation of the Mie scattering with sphere radius follows a similar pattern to that observed in MgO, though slightly more complex. The initial peaks at about 440 and 460  $\text{cm}^{-1}$  broaden and shift to lower frequencies as the particle size increases. Bulk bands around 350 and 372  $\text{cm}^{-1}$  can be seen which grow in intensity and shift to lower frequencies as the particle size increases.

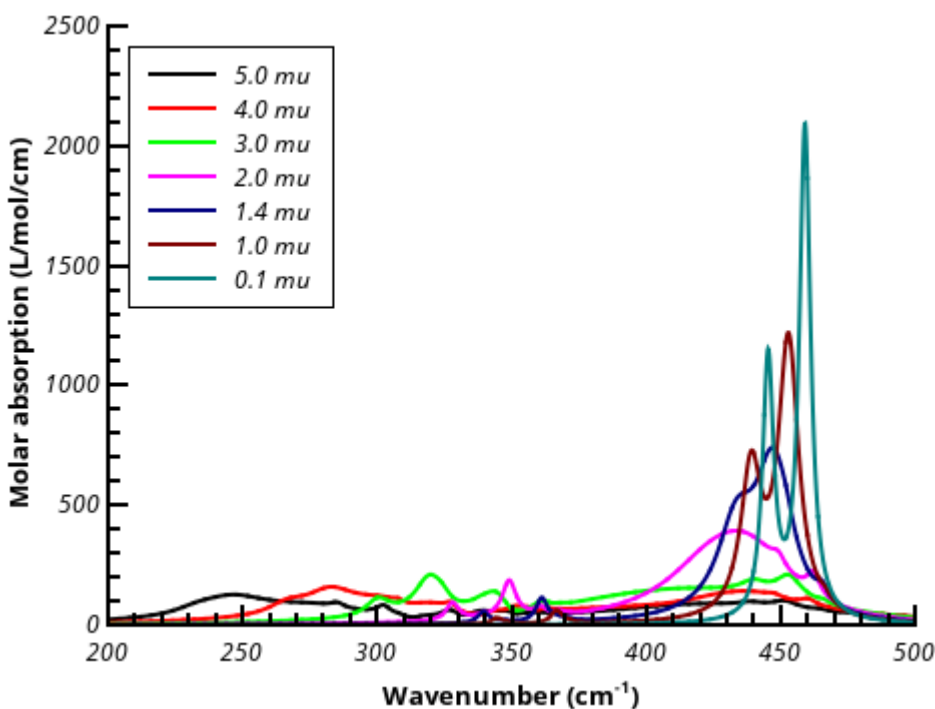


Figure 18: Mie scattering of 10% volume fraction ZnO spheres in PTFE, using a line broadening factor of 5  $\text{cm}^{-1}$ .

## CONCLUSIONS

The PDielec package has been described and examples given as to its application in calculating the infrared absorption spectrum of a dielectric material embedded in supporting matrix. The shape of the crystallites can be taken into account by describing them as spheres, plates, needles or ellipsoids. The package can calculate the dielectric response of the effective medium as well as the infrared absorption as a function of frequency. Several of the examples cover dielectric materials which have been well studied, both experimentally and theoretically and the results are in agreement with the previous work. The package is written in Python and can be extended relatively straightforwardly to interface with other packages. The results show the sensitivity of the absorption spectrum to the particle morphology and illustrate the complexity of interpreting IR and THz absorption spectra.

The PDielec package along with some example test cases for each QM or MM package supported is available on GitHub.<sup>35</sup> The data used to create the figures and tables are openly available from the Leeds University data repository.<sup>58</sup>

## ACKNOWLEDGEMENTS

The authors would like to express their thanks to Professor Sihvola for helpful comments on the manuscript. We would like to thank Lorenzo Maschio who helped with the understanding of the symmetrisation of the hessian needed for the Crystal14 interface.

ADB would also like to acknowledge financial support from both the EPSRC (EP/I026657/1), and the DTRA (US) (HDTRA1-14-C-0013).

## ACKNOWLEDGEMENTS

Citations of the use of this package should use reference<sup>59</sup>

## REFERENCES

- [1] J. Hafner, *J. Comput. Chem.*, 2008, DOI:10.1002/jcc.21057.
- [2] S. J. Clark, M. D. Segall, C. J. Pickard, P. J. Hasnip, M. I. J. Probert, K. Refson, M. C. Payne, *Zeitschrift für Krist.*, 2005, DOI:10.1524/zkri.220.5.567.65075.
- [3] R. Dovesi, R. Orlando, A. Erba, C. M. Zicovich-Wilson, B. Civalleri, S. Casassa, L. Maschio, M. Ferrabone, M. De La Pierre, P. D'Arco, Y. Noel, M. Causa, M. Rerat, B. Kirtman, *Int. J. Quantum Chem.*, 2014, DOI:10.1002/qua.24658.
- [4] X.Gonze, F.Jollet, F.Abreu Araujo, D.Adams, B.Amadon, T.Appelcourt, C.Audouze, J.-M.Beuken, J.Bieder, A.Bokhanchuk, E.Bousquet, F.Bruneval, D.Caliste, M.Cote, F.Dahm, F.Da Pieve, M.Delaveau, M.Di Gennaro, B.Dorado, C.Espejo, G.Geneste, L.Genovese, A.Gerossier, M.Giantomassi, Y.Gillet, D.R.Hamann, L.He, G.Jomard, J.Laflamme Janssen, S.Le Roux, A.Levitt, A.Lherbier, F.Liu, I.Lukacevic,

- A.Martin, C.Martins, M.J.T.Oliveira, S.Ponce, Y.Pouillon, T.Rangel, G.-M.Rignanese, A.H.Romero, B.Rousseau, O.Rubel, A.A.Shukri, M.Stankovski, M.Torrent, M.J.Van Setten, B.Van Troeye, M.J.Verstraete, D.Waroquier, J.Wiktor, B.Xue, A.Zhou, J.W.Zwanziger. Computer Physics Communications 205, 106 (2016).
- [5] P. Giannozzi, et al J.Phys.:Condens.Matter, 21, 395502 (2009) <http://dx.doi.org/10.1088/0953-8984/21/39/395502>.
- [6] Atsushi Togo and Isao Tanaka, Scr. Mater., 108, 1-5 (2015), DOI:10.1016/j.scriptamat.2015.07.021
- [7] J. D. Gale, A. L. Rohl, Mol. Simul., 2003, DOI:10.1080/0892702031000104887.
- [8] J. E. Bertie, Glossary of Terms used in Vibrational Spectroscopy, Handbook of Vibrational Spectroscopy. John Wiley & Sons, Ltd, Chichester, UK, 2006.
- [9] E. B. Wilson, J. C. Decius, P. C. Cross, B. R. Sundheim, Molecular Vibrations: The Theory of Infrared and Raman Vibrational Spectra, Journal of The Electrochemical Society, 102. 235C, 1955.
- [10] T. R. Juliano, T. M. Korter, J. Phys. Chem. A, 2013, DOI:10.1021/jp407112w.
- [11] A. D. Burnett, J. Kendrick, C. Russell, J. Christensen, J. E. Cunningham, A. R. Pearson, E. H. Linfield, A. G. Davies., Anal. Chem., 2013, DOI:10.1021/ac401657r.
- [12] A. Pereverzev, T. D. Sewell, J. Chem. Phys., 2011, DOI:10.1063/1.3518423.
- [13] A. Pereverzev, T. D. Sewell, D. L. Thompson, J. Chem. Phys., 2014, DOI:10.1063/1.4866896.
- [14] H. C. Van De Hulst, in Light Scattering by Small Particles; Dover, New York, 1981.
- [15] F. Wooten, in Optical Properties of Solids; Academic Press, New York, 1972.
- [16] X. Gonze, C. Lee, Phys. Rev. B, 1997, DOI:10.1103/PhysRevB.55.10355.
- [17] H. Fröhlich, in Theory of Dielectrics; Oxford University Press, Oxford, 1948.
- [18] L. Genzel, T. P. Martin, Surf. Sci., 1973, DOI:10.1016/0039-6028(73)90185-4.
- [19] C. J. Serna, M. Ocafia, J. E. Iglesias, J. Phys. C Solid St. Phys., 1987, 20, 473–484.
- [20] J. E. Iglesias, M. Ocana, C. J. Serna, Appl.Spectrosc, 1990, 44, 418–426.
- [21] E. Balan, S. Delattre, D. Roche, L. Segalen, G. Morin, M. Guillaumet, M. Blanchard, M. Lazzeri, C. Brouder, E. K. H. Salje, Phys. Chem. Miner., 2011, DOI:10.1007/s00269-010-0388-x.
- [22] E. Balan, M. Blanchard, J.-F. Hochedepied, M. Lazzeri, Phys. Chem. Miner., 2008, DOI:10.1007/s00269-008-0221-y.
- [23] E. Balan, M. Lazzeri, G. Morin, F. Mauri, Am. Mineral., 2006, DOI:10.2138/am.2006.1922.
- [24] C. Fourdrin, E. Balan, T. Allard, C. Boukari, G. Calas, Phys. Chem. Miner., 2009, DOI:10.1007/s00269-008-0277-8.
- [25] A. Sihvola, in Electromagnetic Mixing Formulas and Applications; P. J. Clarricoats and E. V. Jull, Eds.; IET, The Institution of Engineering and Technology, Michael Faraday House, Six Hills Way, Stevenage SG1 2AY, UK, 1999.

- [26] M. T. Ruggiero, T. Bardon, M. Strlič, P. F. Taday, T. M. Korter, *Phys. Chem. Chem. Phys.*, 2015, DOI:10.1039/C5CP01195G.
- [27] S. Giordano, *J. Electrostat.*, 2003, DOI:10.1016/S0304-3886(02)00199-7.
- [28] T. G. Mackay, A. Lakhtakia, *Opt. Commun.*, 2009, DOI:10.1016/j.optcom.2009.03.035.
- [29] K. Karkkainen, A. Sihvola, K. Nikoskinen, *IEEE Trans. Geosci. Remote Sens.*, 2001, DOI:10.1109/36.921419.
- [30] S. Jamaian, T. G. Mackay, *J. Nanophotonics*, 2010, DOI:10.1117/1.3460908.
- [31] M. Meier and A. Wokaun, *Optics Letters*, 1983, 8, 581-583
- [32] I. Peltoniemi, *J. Quant. Spectroc. Radiat. Transfer*, 1996, 55, 637-647
- [new33] B. J. Sumlin, W. R. Heinson, R. K. Chakrabarty, *J. Quant. Spectrosc. Radiat. Transf.*, 2018, DOI:10.1016/j.jqsrt.2017.10.012.
- [34] B. Stout, M. Nevière, E. Popov, *J. Opt. Soc. Am. A*, **2007**, 24, 1120–1130.
- [35] <http://www.github.com/JohnKendrick/PDielec>
- [36] <http://wiki.scipy.org>
- [37] <https://github.com/yaml>
- [38] <http://xlsxwriter.readthedocs.io/>
- [38] M. Hellenbrandt, *Crystallogr. Rev.*, 2004, DOI:10.1080/08893110410001664882.
- [39] V. G. Tsirelson, A. S. Avilov, Y. A. Abramov, E. L. Belokoneva, R. Kitaneh, D. Feil, *Acta Crystallogr. Sect. B Struct. Sci.*, 1998, DOI:10.1107/S0108768197008963.
- [40] J. P. Perdew, K. Burke, M. Ernzerhof, *Phys. Rev. Lett.*, 1996, DOI:10.1103/PhysRevLett.77.3865.
- [41] G. Kresse, D. Joubert, *Phys. Rev. B*, 1999, DOI:10.1103/PhysRevB.59.1758.
- [42] S. C. Abrahams, J. L. Bernstein, *Acta Crystallogr. Sect. B Struct. Crystallogr. Cryst. Chem.*, 1969, DOI:10.1107/S0567740869003876.
- [43] C. S. McNally, D. P. Turner, A. N. Kulak, F. C. Meldrum, G. Hyett, *Chem. Commun.*, 2012, DOI:10.1039/C2CC14468A.
- [44] K. Yamamoto, C.-D. Tran, H. Shimizu, K. Abe, *J. Phys. Soc. Japan*, 1977, DOI:10.1143/JPSJ.42.587.
- [45] J. L. Rendon, J. E. Iglesias, C. J. Serna, *Opt. Pura Y Apl.*, 1981, 14, 117–122.
- [46] S. Hayashi, N. Nakamori, H. Kanamori, *J. Phys. Soc. Japan*, 1979, DOI:10.1143/JPSJ.46.176.
- [47] D. K. Fisler, J. D. Gale, T. Cygan, Randall, *Am. Mineral.*, 2000, DOI:10.2138/am-2000-0121.
- [48] B. G. Dick, A. W. Overhauser, *Phys. Rev.*, 1958, DOI:10.1103/PhysRev.112.90.
- [49] D. B. DeOliveira, R. A. Laursen, *J. Am. Chem. Soc.*, 1997, DOI:10.1021/ja972270w.
- [50] J.D.H. Donnay, D. Harker, *Am. Mineralogist*, 1937, 22, 446
- [51] C. F. Macrae, I. J. Bruno, J. A. Chisholm, P. R. Edgington, P. McCabe, E. Pidcock, L. Rodriguez-Monge, R. Taylor, J. van de Streek, P. A. Wood, *J. Appl. Crystallogr.*, 2008, DOI:10.1107/S0021889807067908.

- [52] J.M. Hughes, M. Cameron, K.D. Crowley Am. Mineralogist 1989, 74, 870–876
- [53] J. L. Derissen, H. J. Endeman, A. F. Peerdeman, Acta Crystallogr. Sect. B Struct. Crystallogr. Cryst. Chem., 1968, DOI:10.1107/S0567740868004280.
- [54] A. Tkatchenko, M. Scheffler, Phys. Rev. Lett., 2009, DOI:10.1103/PhysRevLett.102.073005.
- [56] T. R. Juliano, T. M. Korter, J. Phys. Chem. A, 2015, DOI:10.1021/jp512359p.
- [57] J. T. Lopez Navarrete, V. Hernandez, F. J. Ramirez, Biopolymers, 1994, DOI:10.1002/bip.360340810.
- [58] John Kendrick and Andrew Burnett (2015): *Dataset associated with PDielec: The Calculation of Infrared and Terahertz Absorption for Powdered Crystals*. University of Leeds.  
<http://doi.org/10.5518/21>
- [59] J. Kendrick, A. Burnett. J. Comput. Chem. 2016, 37, 1491–1504. DOI: 10.1002/jcc.24344